Contrib Mineral Petrol (2015) 169:5
DOI 10.1007/s00410-014-1096-1

ORIGINAL PAPER

Formation and evolution of a Proterozoic magmatic arc: geochemical and geochronological constraints from meta-igneous rocks of the Ongole domain, Eastern Ghats Belt, India

Tapabrato Sarkar · Volker Schenk · Jasper Berndt

Received: 3 July 2014 / Accepted: 8 December 2014 / Published online: 11 January 2015

Abstract Geochemical data and U–Pb zircon results are presented for the intrusive meta-igneous rocks of the Ongole domain, a granulite-facies terrain of the Eastern Ghats Belt in India, with the aim of inferring the tectonic setting and the timing of their formation. Geochemical data suggest that the intrusive meta-igneous rocks (mafic granulites and charnoenderbites) possess trace and rare earth element composition that are typical of magmatic arcs. They are subalkaline, enriched in light rare earth elements and large ion lithophile elements and depleted in heavy rare earth elements and high field strength elements like Nb, Ta and Ti. These characteristics indicate that the primary magmas of these rocks were derived by partial melting of a depleted mantle wedge that had been metasomatized by a slab component. Zircon grains collected from five charnoenderbites are large and euhedral to subhedral and display fine-scale oscillatory growth zoning in CL images, implying a magmatic origin. The grains frequently show narrow-to-broad unzoned overgrowths, implying a metamorphic origin. The oscillatory-zoned cores yield Paleoproterozoic concordia ages of ca. 1,750–1,710 Ma, interpreted as the time of magma emplacement. The unzoned overgrowths yield very late Paleoproterozoic ages of ca. 1,630–1,600 Ma, interpreted as the timing of metamorphism. An enderbite showing both magmatic and metamorphic concordia ages of ca. 1,605 Ma points to the existence of syn-metamorphic intrusions. Together, the presented geochemical and geochronological evidence suggests that the Ongole domain was a magmatic arc near the Indian continent during the Paleoproterozoic. Subsequently, the rocks were metamorphosed during the late Paleoproterozoic, and the terrain was accreted to the Indian craton during the early Mesoproterozoic. The formation and growth of the Ongole domain magmatic arc through subduction-related accretion can be correlated with the growth of Columbia (1.8–1.2 Ga), but its accretion to the Indian craton is apparently unrelated to the formation of any supercontinent on a global scale.

Keywords Eastern Ghats Belt · Ongole domain · Geochemistry · LA-ICP-MS zircon geochronology · Columbia supercontinent

Communicated by Othmar Müntener.

Electronic supplementary material The online version of this article (doi:10.1007/s00410-014-1096-1) contains supplementary material, which is available to authorized users.

T. Sarkar (✉) · V. Schenk
Institute for Geosciences, University Kiel, 24118 Kiel, Germany
e-mail: tapabrato@gmail.com

J. Berndt
Institute for Mineralogy, University Münster, Correnstrasse 24, 48149 Münster, Germany

Introduction

The formation and subsequent evolution of continental crust from the Archean to the present is one of the key topics in earth sciences that is widely debated (Condie 2000; Hawkesworth and Kemp 2006; Arndt 2013). Continental crust grew mainly along subduction zones of active continental margins by tectonic accretion and emplacement of juvenile magmatic rocks besides minor magmatism in intra-plate tectonic settings (Şengör et al. 1993; Jagoutz et al. 2007; Windley and Garde 2009), though the nature of geodynamic processes that generated Archean continental crust still remains controversial (Polat 2012 and references therein). Trace element similarities, such as enrichment of

light rare earth elements (LREE), depletion of Nb, Ta and Ti and enrichment of Pb with respect to REE, between Proterozoic magmatic sequences and volcanic rocks at modern subduction zones imply that post-Archean continental crust formed in a similar way as in the Phanerozoic (Taylor and McLennan 1985; Rudnick 1995; Cawood et al. 2006). Magmatic arcs have always been important entities in models of continental growth and preserve unique geochemical characteristics (Polat 2012) and tectono-metamorphic histories (Sarkar et al. 2014). They are often formed during the process of continental amalgamation through the subduction of the intervening oceanic lithosphere in a prolonged subduction–accretion–collision regime (Korsch et al. 2011).

The Ongole domain in the southern part of the Eastern Ghats Belt exposes a variety of granulite-facies rocks mainly dominated by intermediate (enderbite) to felsic (charnockite) granulites, collectively referred to as charnoenderbites (Dobmeier and Raith 2003; Sarkar and Schenk 2014). Geochemical data from discrete magmatic bodies around and within the Ongole domain indicate their formation in a continental arc setting (Dharma Rao and Santosh 2011). However, a systematic geochemical and geochronological study of the now granulite-facies meta-igneous rocks of the Ongole domain itself has not yet been undertaken.

In this contribution, we present field relationships, trace and rare earth element geochemistry and U–Pb zircon (LA-ICPMS) geochronological data of the meta-igneous rocks of the Ongole domain (mostly charnoenderbites and some associated mafic granulites). Our data constrain the timing and tectonic setting of crust formation: The Ongole domain was formed in a continental arc setting during a short time interval of the late Paleoproterozoic. The geochronological data further constrain the timing of metamorphism. This study reconstructs the history of a magmatic arc from its growth via subduction-related accretion to its attachment with the craton and provides new insights into the evolution of Proterozoic continental crust in Peninsular India.

Geological setting

The Eastern Ghats Belt (EGB), which includes the Ongole domain, is a Proterozoic crustal segment extending for ca. 1,000 km along the eastern margin of the Indian peninsula in a NE–SW direction (Fig. 1). It is an assembly of intensely deformed, polymetamorphosed and deeply eroded high-grade terrains bounded to the west along several shear zones by the Archean cratons of the Indian shield (for summary see Dobmeier and Raith 2003).

Earlier subdivisions of the EGB were based on lithology (Ramakrishnan et al. 1998) and isotopic signatures (Rickers et al. 2001). Dobmeier and Raith (2003) divided the EGB into four crustal provinces, which were further divided into crustal domains based on their distinct geological histories and separated from each other by tectonic boundaries. The Krishna Province in the southern part of the EGB comprises the granulite-facies Ongole domain and the medium-to-low-grade Vinjamuru and Udayagiri domains (Fig. 1). The present work is focused on the Ongole domain that lies in between the Archean Eastern Dharwar craton to the west and the Mesoproterozoic Eastern Ghats Province to the east (Fig. 1).

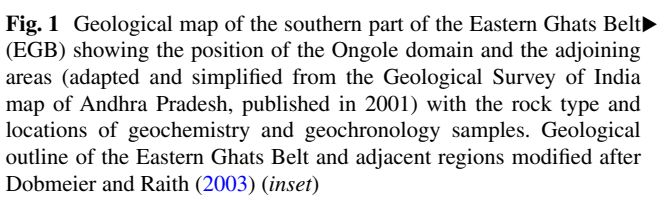

Fig. 1 Geological map of the southern part of the Eastern Ghats Belt (EGB) showing the position of the Ongole domain and the adjoining areas (adapted and simplified from the Geological Survey of India map of Andhra Pradesh, published in 2001) with the rock type and locations of geochemistry and geochronology samples. Geological outline of the Eastern Ghats Belt and adjacent regions modified after Dobmeier and Raith (2003) (*inset*)

The Ongole domain is characterized by large volumes of multi-intrusive charnoenderbites with enclaves of migmatitic metasedimentary rocks from meter to outcrop scale (Dobmeier and Raith 2003; Sarkar and Schenk 2014). Geochemical data of the small Kondapalle mafic–ultramafic complex within the northern part of the Ongole domain have been interpreted as indications for a formation in a magmatic arc setting (Dharma Rao and Santosh 2011). A preliminary study revealed that charnoenderbites were emplaced at ca. 1.7 Ga (Kovach et al. 2001). The Nd model ages (T_{DM}) of 2.5–2.3 Ga from the charnoenderbites suggest a mantle-derived magma with substantial input of Archean crustal material (Rickers et al. 2001). This was followed by a high-grade metamorphic event at ca. 1.6 Ga (Simmat and Raith 2008; Bose et al. 2011; Sarkar et al. 2014), indicating that the Ongole domain is dominantly a Paleoproterozoic terrain.

Field relations show that the mafic–ultramafic complex near Kondapalle has been intruded and dismembered by charnoenderbites (Sengupta et al. 1999) that were thought to have been emplaced at 1.7 Ga. The emplacement of the same mafic–ultramafic complex has been dated at 1.69–1.63 Ga (Dharma Rao et al. 2012) indicating different generations of magmatic rocks in the area. An N–S array of a suite of rift-related alkaline rocks ranging from quartz syenite to alkali granite marks the boundary between the Ongole domain and the Eastern Dharwar craton (Fig. 1; Upadhyay 2008).

The amphibolites-facies Vinjamuru domain, adjacent to the southwestern part of the Ongole domain (Fig. 1), is essentially composed of felsic to intermediate metavolcanic rocks in addition to some metasediments and granitoids (see Dobmeier and Raith 2003). Zircon dating of the metavolcanic rocks from the northern part of the Vinjamuru domain points to a major magmatic activity in the

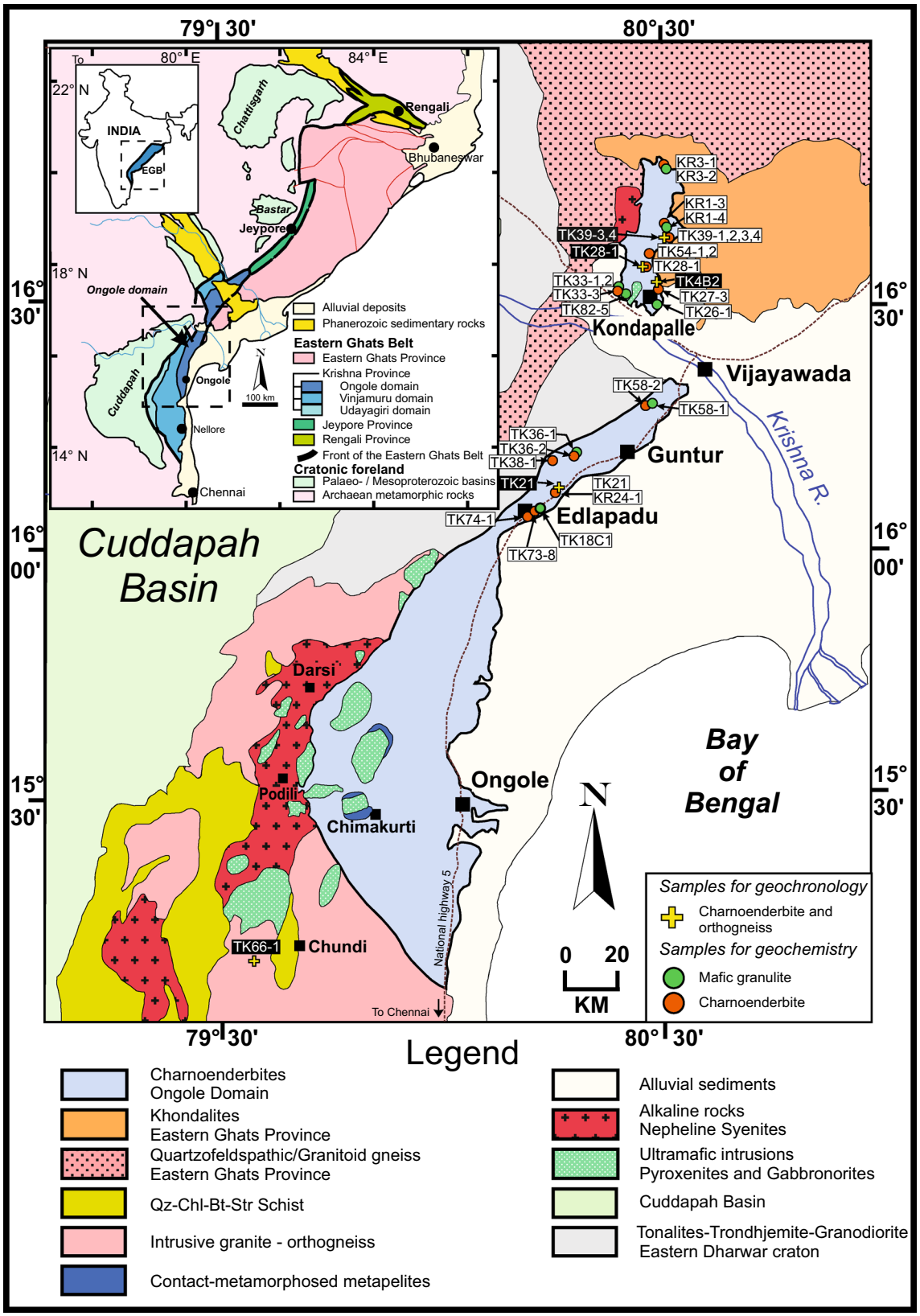
79° 30'
80° 30'
16° 30'
16° 00'
15° 30'
To
80° E
84° E
22° N
18° N
14° N
INDIA
EGB
Chattisgarh
Rengali
Bhubaneswar
Bastar
Jeypore
Ongole domain
Cuddapah
Ongole
Nellore
Chennai
100 km
Alluvial deposits
Phanerozoic sedimentary rocks
Eastern Ghats Belt
Eastern Ghats Province
Krishna Province
Ongole domain
Vinjamuru domain
Udayagiri domain
Jeypore Province
Rengali Province
Front of the Eastern Ghats Belt
Cratonic foreland
Palaeo- / Mesoproterozoic basins
Archaean metamorphic rocks
Cuddapah Basin
Kondapalle
Vijayawada
Guntur
Edlapadu
Krishna R.
Darsi
Podili
Chimakurti
Ongole
Chundi
National highway 5
To Chennai
Bay of Bengal
N
0 20
KM
KR3-1
KR3-2
KR1-3
KR1-4
TK39-3,4
TK39-1,2,3,4
TK28-1
TK54-1,2
TK28-1
TK33-1,2
TK33-3
TK4B2
TK27-3
TK82-5
TK26-1
TK58-2
TK58-1
TK36-1
TK36-2
TK38-1
TK21
TK21
KR24-1
TK74-1
TK18C1
TK73-8
TK66-1
Samples for geochronology
Charnoenderbite and orthogneiss
Samples for geochemistry
Mafic granulite
Charnoenderbite
Legend
Charnoenderbites Ongole Domain
Khondalites Eastern Ghats Province
Quartzofeldspathic/Granitoid gneiss Eastern Ghats Province
Qz-Chl-Bt-Str Schist
Intrusive granite - orthogneiss
Contact-metamorphosed metapelites
Alluvial sediments
Alkaline rocks Nepheline Syenites
Ultramafic intrusions Pyroxenites and Gabbronorites
Cuddapah Basin
Tonalites-Trondhjemite-Granodiorite Eastern Dharwar craton

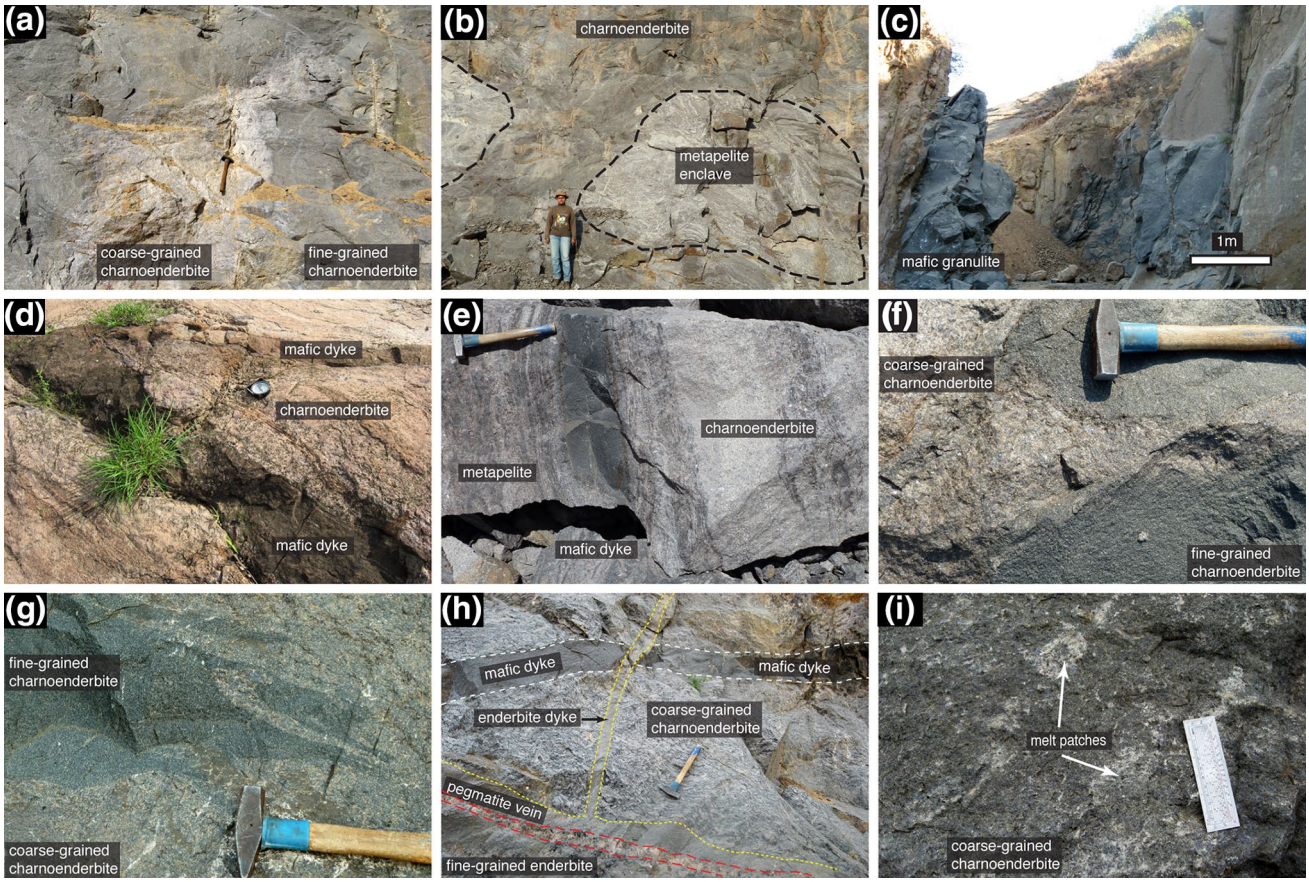

Fig. 2 **a** Coarse-grained charnoenderbite intruding into fine-grained charnoenderbite; **b** enclaves of metapelitic granulite within charnoenderbite; **c** mafic granulite associated with charnoenderbite; **d** charnoenderbite cut by a mafic dyke; **e** metapelitic enclave cut by mafic dyke near the contact of metapelite and charnoenderbite; **f**, **g** contact between coarse-grained and fine-grained charnoenderbites; **h** interrelation among the different generations of magmatic rocks. A charnockite (1) has been intruded by a mafic dyke (2) and a fine-grained enderbite (3). A pegmatite vein (4) has cut through all the rock units (Sarkar and Schenk 2014); **i** leucosome patches within charnoenderbite

Paleoproterozoic (ca. 1.78 Ga, Ravikant et al. 2013), followed by amphibolite facies metamorphism at 1.61 Ga (Sarkar et al. 2014). From geochemical data, the rocks are interpreted to have formed in a continental magmatic arc tectonic setting (Ravikant et al. 2013).

Field relationships and petrography

The Ongole domain is dominantly composed of large volumes of charnoenderbites (Fig. 2a). It covers a substantial part of the Ongole domain. The metapelitic granulites constitute only a small portion (<10 vol%) of the exposed rocks and occur as enclaves (Fig. 2b) within the charnoenderbites and have sharp contacts with the host rock. They are migmatitic showing prominent layers of leucosome and melanosome ranging from centimeter to decimeter scale, mostly deformed (Sarkar and Schenk 2014). Compositionally, they are Fe–Al-rich granulites with garnet, sillimanite, spinel, orthopyroxene, cordierite, K-feldspar, plagioclase and quartz as the most common phases. The mafic rocks are rare and form enclaves, dykes and xenoliths within the charnoenderbites (Fig. 2c, d, e) and as a separate layered mafic intrusion in the northern part of the Ongole domain near Kondapalle. All the rocks are exposed along freshly cut quarry faces throughout the Ongole domain.

The charnoenderbites have a homogeneous and massive appearance in outcrops. Field observation reveals that the enderbites are generally fine-grained massive to medium-grained gneissic rocks whereas the charnockites are generally medium- to coarse-grained gneissic to pegmatoidal (Fig. 2a, f, g). However, the gneissic nature is clearly observed only on weathered surfaces. Complex crosscutting relationships among the different varieties of rocks are preserved in outcrops, indicating multiple stages of intrusion (Fig. 2h).

The rocks are composed of a quartzofeldspathic matrix together with garnet, orthopyroxene, biotite and ilmenite. The relative proportions of K-feldspar and plagioclase vary considerably depending on the rock type with K-feldspar

dominating in the felsic varieties (charnockites), while plagioclase is dominant in the intermediate varieties (enderbites). The rocks underwent granulite-facies (ca. 900 °C) metamorphic events and migmatization, which is also evident from the thin leucosome patches (Fig. 2i). It is, however, not clear whether orthopyroxene is a product of this metamorphism or inherited from the magmatic protolith. However, garnet is a metamorphic mineral in these charnoenderbites, as it contains monazite preserving metamorphic ages (ca. 1,600 Ma) and not magmatic ages (ca. 1,720 Ma). Further details of field relationships, mineral assemblages and petrography of all the different rock types are discussed in Sarkar and Schenk (2014).

Analytical techniques

Geochemistry

A representative part of each sample was washed with distilled water and crushed to a very fine powder in an agate mill at the Institute for Geosciences, University of Kiel. Major element concentrations of whole rocks were obtained from XRF analyses at the University of Kiel by analyzing glass disks with a Phillips PW 1,400 X-ray fluorescence analyzer. Fused glass disks were prepared by mixing 0.6 g of sample powder with 3.6 g of $Li_2B_4O_7$ and 2 g of NH_4NO_3 (flux), followed by melting in an OXIFLUX 5-stage burner.

Trace and rare earth element analyses were carried out at GeoForschungsZentrum (GFZ) in Potsdam, Germany. Trace element concentrations were determined by Inductively Coupled Plasma Mass Spectrometry (ICP-MS) using a VG Plasma Quad PG2. Sample powders were decomposed using HF, Aqua regia and $HClO_4$ in pressure vessels. The decomposed samples were dissolved in HNO_3 and diluted to a volume of 50 ml for analysis. Rare earth elements (REE) and *Y* contents were determined by inductively coupled plasma-atomic emission spectroscopy (ICP-AES) following the procedure of Zuleger and Erzinger (1988). The samples were decomposed and dissolved using the Na_2O_2 sinter method, and the REE were separated and concentrated using ion-exchange methods. The standards GM, JG-3, GSR-1 and JG-1a (Govindaraju 1994) were prepared and analyzed together with the unknown samples. The accuracy of each analysis was assessed by comparing the standards with certified values (Liang and Grégoire 2000; Dulski 2001) and estimated to be better than 10 % for each element.

U–Pb zircon geochronology by LA-ICP-MS

Zircon grains were separated from hand specimens by standard heavy mineral separation techniques. The rocks (hand specimen size) were first crushed followed by magnetic separation using a hand magnet and a Franz isodynamic magnetic separator to exclude the magnetic minerals. The separate was then subjected to heavy mineral separation using bromoform liquid. To include all the varieties of zircon grains in terms of shape and size, the individual zircon grains were carefully hand picked from the heavy mineral residue. Selected grains were mounted on epoxy resin disks and polished. To study their internal structure, the polished mounts were photographed and cathodoluminescence (CL) images were obtained before analyses using the JEOL JSM-6490 Scanning Electron Microscope at the Institute for Geosciences, University of Frankfurt. Points were carefully selected on several zircon grains to include all petrographically distinct domains under CL images. U–Pb isotopic analyses were carried out by using a Element2 sector field ICP-MS coupled to a New Wave UP193HE ArF Excimer laser system at the Institute for Mineralogy of the University of Münster. The analytical details for the measurement of U and Pb isotopes using the LA-ICP-MS are further elaborated by Kooijman et al. (2012). Two zircon reference materials were used: GJ-1 (Jackson et al. 2004) was the regular primary standard reference during the sessions, and 91500 zircon (Wiedenbeck et al. 1995) was utilized as an unknown to monitor precision and accuracy. Analysis ($n = 18$) of the 91500 standard reference zircon over the course of this study yielded values of 0.1783 (±2.1 %, 2σ) for the $^{206}Pb/^{238}U$, 0.0749 (±2.3 %, 2σ) for $^{207}Pb/^{206}Pb$ and 1.842 (±3.2 %, 2σ) for the $^{207}Pb/^{235}U$ ratios (Table 3 in electronic appendix) and match within error the values reported in Wiedenbeck et al. (1995).

Geochemistry

Alteration and element mobility

The meta-igneous rocks of the Ongole domain have undergone granulite-facies metamorphism. Therefore, fresh samples were carefully selected, and large samples (roughly 10–12 cm cubes) were crushed to assure representative compositions. Altogether, a total of 28 samples are selected forming the basis of all subsequent discussions.

The coherent patterns in the chondrite and primitive mantle-normalized rare earth and trace element plots indicate that the primary magmatic compositions, at least for REE and HFSE, are largely preserved. This is supported by the apparent positive correlation between Zr and several REE and HFSE (Fig. A1 in electronic appendix).

Rock classification

In order to apply a coherent nomenclature based on widely used rock classification schemes, the magmatic rocks of

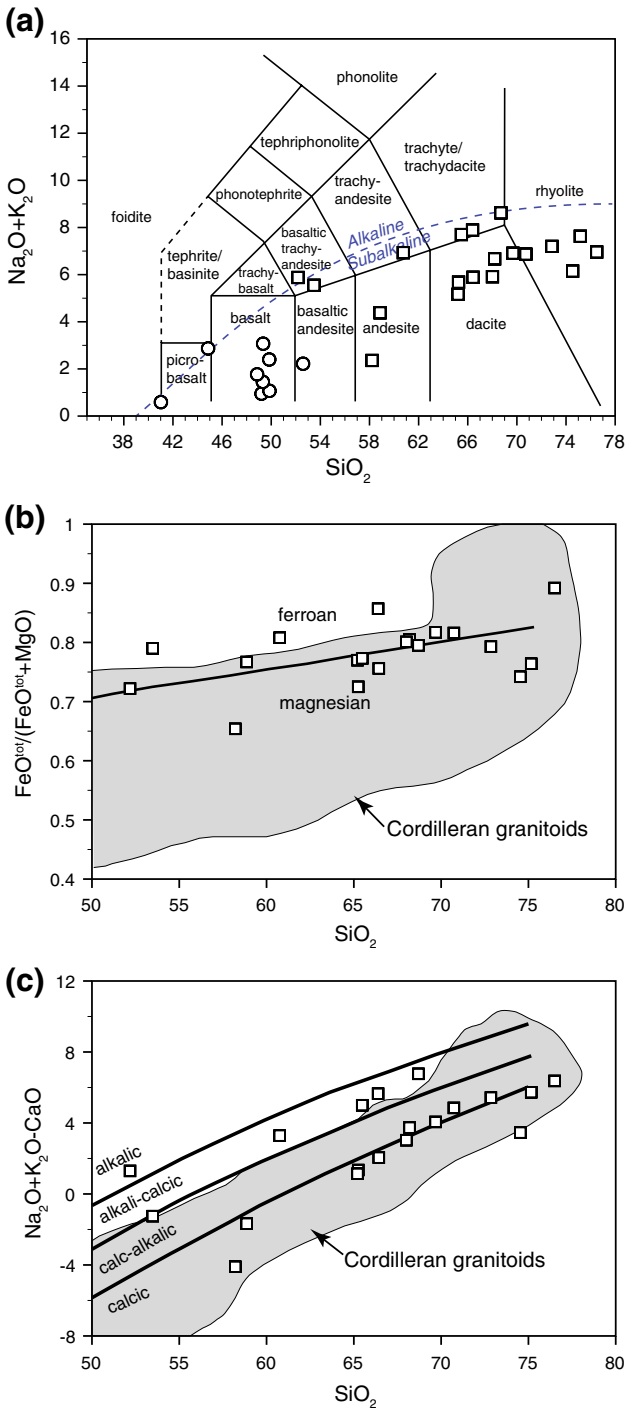

Fig. 3 **a** Classification of magmatic rocks of the Ongole domain on the total alkali vs. SiO_2 (TAS) diagram of Irvine and Baragar (1971). All samples show subalkaline affinity. The mafic granulites are represented by *circles,* and the charnoenderbites are represented by *squares*; **b** and **c** $FeO^{tot}/(FeO^{tot})+MgO$ and K_2O $+Na_2O$-CaO (MALI: modified alkali-lime index) versus SiO_2 plots. The composition fields of Cordilleran-type granites as well as **b** the boundary between ferroan and magnesian plutons and **c** the ranges of alkalic, alkali-calcic, calc-alkalic and calcic rock series are from Frost et al. (2001)

the Ongole domain are plotted in the total alkalis against SiO_2 (TAS) classification diagram (Fig. 3a; Le Bas et al. 1986). The boundary line between alkaline and subalkaline series is from Irvine and Baragar (1971). The rocks plot in the subalkaline series and range from the field of basalt to rhyolite. On this diagram, nine samples plot in the field of basalt, picro basalt and basaltic andesite. From now onwards, these nine samples will be referred to as mafic granulites. Out of the remaining 19 samples, 14 samples plot in the field of dacite, trachydacite and rhyolite, two each in the field of basaltic trachyandesite and andesite and one in the field of trachyandesite. Henceforth, all of these 19 samples, ranging from intermediate to acidic in composition, will be referred to as charnoenderbites. There are six charnoenderbite samples lying near the alkaline–subalkaline boundary and seem to be shifted toward higher alkali contents (Fig. 3a), indicating that alkali elements in these samples might have been mobile during granulite-facies metamorphism.

According to the plot of Fe* [Fe* = $FeO^{tot}/(FeO^{tot}$ + MgO)] and weight percent SiO_2 (Fig. 3b; Frost et al. 2001), that is used to classify granitoid rocks into magnesian and ferroan types, the charnoenderbites plot around the boundary of magnesian and ferroan. In terms of the modified alkali-lime index (MALI) plot (Fig. 3c) by Frost et al. (2001), the charnoenderbites are mostly calcic to calc-alkalic. Only six samples are alkali-calcic to alkalic. These are the same samples that are shifted due to higher alkali contents in the TAS diagram (Fig. 3a). This interpretation is supported by Fig. 4d (K_2O vs. SiO_2) where K_2O in the same six samples is higher than in all other charnoenderbites with similar SiO_2 contents. The higher K_2O contents are also the reason that they follow the alkali-calcic to alkalic trend instead of calcic to calc-alkalic trend as all the other charnoenderbites. In all other major and trace element plots and in the trace element patterns (see below), they are not distinguishable from the other charnoenderbites. This leads us to assume that enrichment of fluid mobile element potassium is due to a metasomatic process. The compositional range of Cordilleran granitoids is shown (Fig. 3b, c), which demonstrates that the charnoenderbites have compositions similar to the Cordilleran granitoids of the USA.

Major and trace element composition

Mafic granulites Major and trace element compositions of the mafic granulites from the Ongole domain are presented in Table 1. The samples have SiO_2 = 44.9–52.6 wt%, TiO_2 = 1.0–2.1 wt%, total Fe_2O_3 = 13.1–18.4 wt%, MgO = 6.2–7.6 wt%, Al_2O_3 = 13.2–15.0 wt%, CaO = 7.5–10.8 wt% and Na_2O + K_2O = 1.0–3.1 wt%. Mg#, calculated as 100 $Mg^{2+}/(Mg^{2+}+Fe^{2+}_{tot})$, varies from 40.8 to 48.8.

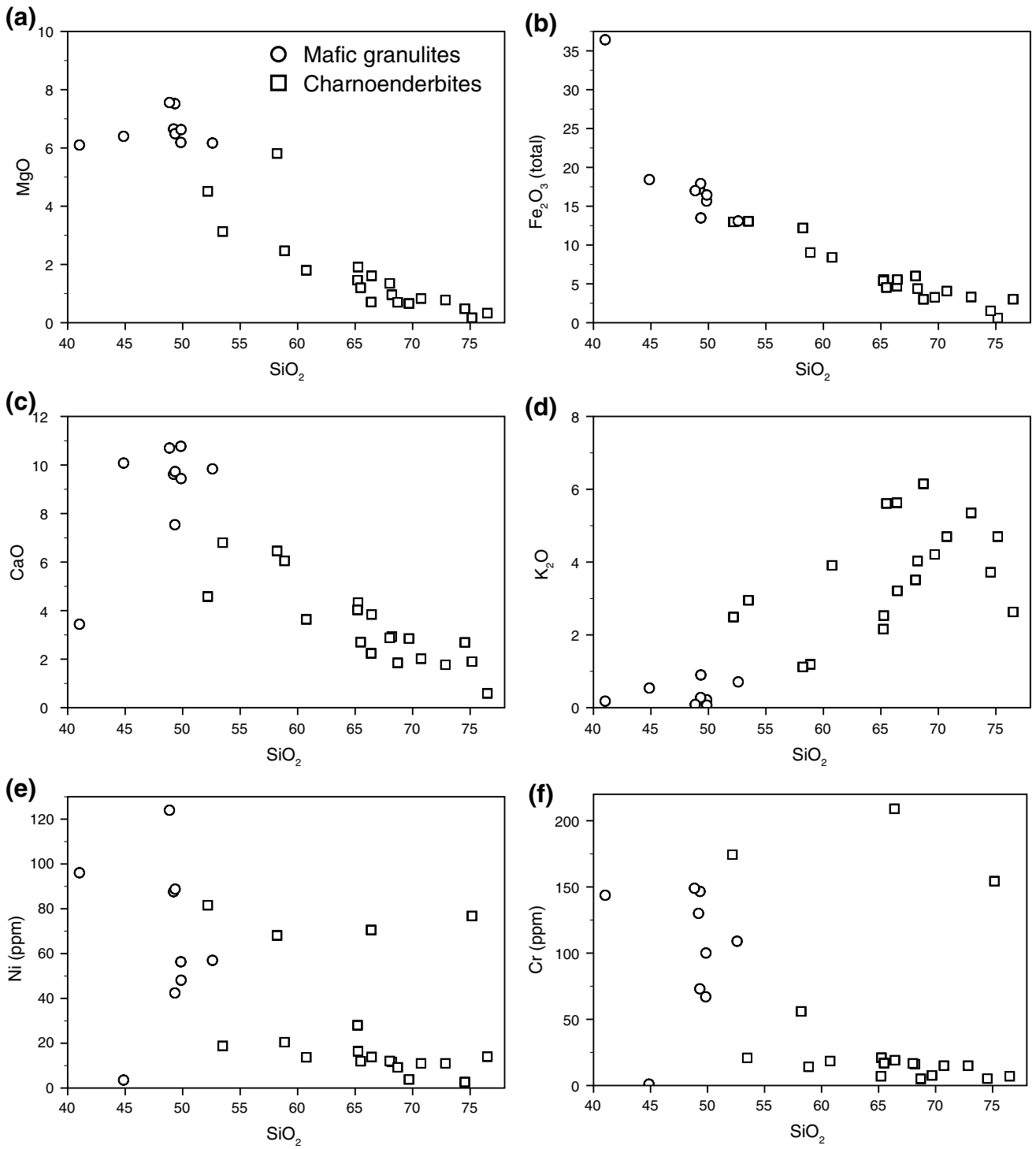

Fig. 4 SiO_2 vs. selected major and trace element variation diagram for the rocks of the Ongole domain

One sample (TK18C1) with a picro basalt chemistry has lower SiO_2 (41.0 wt%), Al_2O_3 (8.11 wt%), CaO (3.4 wt%), $Na_2O + K_2O$ (0.59 wt%), Mg# (23.9) and higher total Fe_2O_3 (36.43 wt%) than the above-mentioned range. Major and trace element variation diagrams of selected elements (Fig. 4) show that SiO_2 is negatively correlated with MgO, total Fe_2O_3, CaO, Ni and Cr and positively correlated with K_2O.

The mafic granulites have low Sr contents (6–284 ppm, average 114 ppm) and high *Y* contents (26–39 ppm,

Table 1 Major (wt%) and trace (ppm) element composition for the meta-igneous rocks of the Ongole domain

Sample	Mafic granulites									Charnoenderbites				
	TK18-C1	TK26-1	TK33-1	TK33-2	TK36-1	TK58-1	TK82-5	KR1-4	KR3-2	TK27-3	TK39-1	TK39-2	TK39-3	TK39-4
SiO_2	41.02	49.21	49.34	49.84	49.86	44.86	49.32	52.59	48.85	60.75	65.48	58.86	66.39	68.19
Al_2O_3	8.11	13.98	14.70	13.15	14.99	13.84	13.68	14.48	13.49	15.76	15.13	16.37	14.50	14.52
Fe_2O_3 (t)	36.43	17.19	13.49	15.66	16.45	18.43	17.91	13.10	17.00	8.41	4.53	9.04	4.71	4.39
MgO	6.10	6.65	6.49	6.19	6.63	6.40	7.52	6.17	7.56	1.80	1.20	2.47	0.71	0.96
CaO	3.44	9.62	9.73	10.77	9.44	10.08	7.54	9.84	10.70	3.64	2.70	6.05	2.24	2.93
Na_2O	0.41	0.88	2.17	2.18	1.00	2.33	1.17	1.51	1.68	3.02	2.09	3.19	2.26	2.64
K_2O	0.18	0.07	0.90	0.22	0.07	0.54	0.28	0.71	0.09	3.91	5.61	1.19	5.63	4.03
TiO_2	1.41	1.87	1.88	1.19	1.00	2.07	1.07	1.29	1.62	1.07	0.63	1.05	1.09	0.56
P_2O_5	0.15	0.22	0.57	0.11	0.07	0.24	0.12	0.13	0.14	0.42	0.18	0.41	0.30	0.18
MnO	1.81	0.22	0.18	0.23	0.30	0.25	0.38	0.20	0.19	0.10	0.05	0.10	0.07	0.06
LOI	0.11	0.12	0.10	0.16	0.21	0.31	0.24	n.d	n.d	0.12	0.50	0.40	0.16	0.45
Total	99.17	100.03	99.55	99.70	100.02	99.35	99.23	100.02	101.32	99.00	98.10	99.13	98.06	98.91
FeO (t)	34.62	15.49	12.15	14.11	14.82	16.60	16.14	11.80	15.32	7.58	4.08	8.14	4.24	3.95
Mg#	24	43	49	44	44	41	45	48	47	30	34	35	23	30
$Na_2O + K_2O$	0.59	0.95	3.07	2.40	1.07	2.87	1.45	2.22	1.77	6.93	7.70	4.38	7.89	6.67
FeO/(FeO+MgO)	0.85	0.70	0.65	0.70	0.69	0.72	0.68	0.66	0.67	0.81	0.77	0.77	0.86	0.80
$Na_2O + K_2O$–CaO	−2.85	−8.67	−6.66	−8.37	−8.37	−7.21	−6.09	−7.62	−8.93	3.29	5.00	−1.67	5.65	3.74
Cs	0.678	0.000	0.300	0.000	0.000	0.604	0.030	0.573	0.478	0.162	0.398	0.216	0.018	0.275
Rb	22.2	0.3	22.0	1.2	0.7	26.9	2.6	34.6	3.6	166.8	218.8	52.5	33.5	180.7
Ba	130	79	570	76	47	166	145	123	37	639	2,736	856	1,117	556
Sr	7	91	284	139	95	132	89	62	128	140	365	472	198	109
Pb	0.9	1.2	7.0	2.2	3.6	44.9	4.9	7.2	1.7	17.5	23.9	10.4	3.9	18.8
Th	0.6	1.7	3.6	0.4	2.2	4.0	0.9	3.0	2.0	26.0	18.1	2.2	2.5	48.4
U	0.42	0.26	0.80	0.12	2.15	0.82	0.16	1.87	0.53	0.93	0.94	0.42	0.51	0.88
Zr	31.4	35.2	38.0	23.4	44.2	64.5	28.9	77.0	98.0	167.3	226.2	88.2	48.3	148.6
Ta	0.41	0.63	0.59	b.d.l	0.56	1.28	0.44	0.96	0.63	1.10	0.59	0.58	0.98	0.80
Y	36.0	37.0	26.0	32.0	26.0	39.0	26.0	31.4	29.9	68.0	11.0	25.0	35.0	24.0
Nb	5.70	8.37	10.00	1.31	5.40	7.57	5.70	5.87	6.03	32.48	11.86	13.96	13.68	21.28
Sc	17.0	52.2	32.6	49.4	45.7	7.5	46.7	38.0	52.0	20.0	9.0	19.4	50.6	9.2
Cr	143.7	130.0	146.6	67.0	100.1	1.1	73.0	109.0	149.0	18.5	16.9	14.2	209.1	16.1
Ni	96.09	87.63	88.79	56.34	48.12	3.57	42.43	57.00	124.00	13.72	11.96	20.46	70.54	11.65
Co	35.34	53.56	46.51	49.97	55.24	8.05	47.20	26.00	67.00	15.62	9.70	19.07	58.17	8.83
V	101.8	378.8	230.2	316.5	279.0	35.5	313.6	311.0	397.0	97.9	102.0	153.9	323.1	49.3
Ga	9.9	20.4	16.1	15.1	16.3	17.8	15.5	13.0	16.0	21.0	16.4	20.5	19.0	17.0

Table 1 continued

Sample	Mafic granulites									Charnoenderbites				
	TK18-C1	TK26-1	TK33-1	TK33-2	TK36-1	TK58-1	TK82-5	KR1-4	KR3-2	TK27-3	TK39-1	TK39-2	TK39-3	TK39-4
Zn	210.42	78.55	87.48	92.64	151.49	59.98	119.90	123.00	142.00	55.78	44.98	88.48	139.37	39.69
Cu	1,426	74	29	49	60	13	28	n.d	309	28	24	73	70	19
La	12.0	13.0	23.0	4.1	10.0	14.0	9.1	12.7	6.2	79.0	37.0	46.0	293.0	79.0
Ce	24.0	34.0	47.0	9.9	22.0	34.0	20.0	28.6	15.8	161.0	66.0	97.0	665.0	155.0
Pr	2.3	4.6	5.7	1.3	2.6	4.4	2.4	3.7	2.4	18.0	7.1	11.0	77.0	17.0
Nd	9.9	23.0	26.0	8.1	12.0	21.0	11.0	14.5	11.5	70.0	26.0	46.0	274.0	62.0
Sm	3.10	6.10	5.80	3.00	3.30	5.60	3.10	4.53	4.59	14.00	4.70	8.70	30.00	9.90
Eu	1.10	1.40	2.00	1.20	1.10	1.90	1.10	1.10	1.10	1.50	2.00	2.00	1.80	1.40
Gd	4.90	6.80	5.90	4.30	4.00	6.50	3.80	4.57	4.61	14.00	3.70	7.30	16.00	8.00
Tb	0.93	1.20	0.97	0.84	0.77	1.20	0.76	0.83	0.84	2.30	b.d.l	1.10	1.90	1.10
Dy	6.10	7.20	5.20	5.60	4.80	7.20	4.70	5.56	5.49	14.00	2.30	5.20	8.80	5.50
Ho	1.20	1.40	0.99	1.20	0.95	1.40	0.94	1.16	1.11	2.60	0.44	0.99	1.40	0.96
Er	3.70	4.30	2.90	3.80	3.00	4.40	3.00	3.26	3.10	6.40	1.10	2.60	3.40	2.40
Tm	0.52	0.59	0.36	0.55	0.44	0.65	0.45	0.49	0.47	0.85	b.d.l	0.37		0.35
Yb	3.30	3.90	2.60	3.70	2.90	4.20	3.00	3.31	3.09	4.50	0.99	2.20	2.80	1.90
Lu	0.47	0.56	0.38	0.55	0.43	0.62	0.44	0.48	0.46	0.60	0.16	0.32	0.38	0.28
Eu/Eu*	0.86	0.66	1.04	1.02	0.92	0.96	0.98	0.74	0.73	0.33	1.46	0.77	0.25	0.48
K	1,494	581	7,471	1,826	581	4,483	2,324	5,894	747	32,458	46,570	9,879	46,736	33,454
Ti	8,402	11,143	11,203	7,091	5,959	12,335	6,376	7,687	9,654	6,376	3,754	6,257	6,495	3,337
P	655	960	2,488	480	306	1,048	524	567	611	1,833	786	1,789	1,309	786
Sr/Y	0.19	2.47	10.92	4.35	3.66	3.38	3.43	1.97	4.28	2.06	33.22	18.87	5.65	4.55
Th/Yb	0.19	0.42	1.38	0.12	0.77	0.95	0.31	0.90	0.66	5.79	18.27	1.02	0.91	25.47
Ta/Yb	0.12	0.16	0.23	b.d.l	0.19	0.30	0.15	0.29	0.20	0.24	0.59	0.26	0.35	0.42
Nb/Y	0.16	0.23	0.38	0.04	0.21	0.19	0.22	0.19	0.20	0.48	1.08	0.56	0.39	0.89
Y + Nb	n.d	n.d	n.d	n.d	n.d	n.d	n.d	n.d	n.d	100.48	22.86	38.96	48.68	45.28
Nb/La_{PM}	0.46	0.62	0.42	0.31	0.52	0.52	0.60	0.45	0.94	0.40	0.31	0.29	0.04	0.26
Zr/Nd_{PM}	0.38	0.19	0.18	0.35	0.45	0.37	0.32	0.64	1.03	0.29	1.05	0.23	0.02	0.29
La/Yb_{CN}	2.47	2.26	6.01	0.75	2.34	2.26	2.06	2.60	1.36	11.93	25.39	14.20	71.09	28.25
Tb/Yb_{CN}	1.26	1.37	1.66	1.01	1.18	1.27	1.13	1.11	1.21	2.28	0.00	2.23	3.03	2.58
DF1	−1.03	−1.71	−1.95	−4.09	−3.21	−3.56	−1.69	−3.43	−2.87	n.d	n.d	n.d	n.d	n.d
DF2	1.64	0.21	−1.40	0.86	−0.41	−0.91	1.02	−0.93	−0.28	n.d	n.d	n.d	n.d	n.d

Table 1 continued

Sample	Charnoenderbites													
	TK54-1	TK54-2	TK74-1	TK 73-8	TK38-1	TK28-1	TK33-3	KR1-3	KR3-1	KR24-1	KR11-1	TK 36-2	TK 21	TK 58-2
SiO2	68.01	69.68	65.25	58.21	53.48	68.70	52.18	65.21	76.50	72.85	70.73	74.54	66.43	75.16
AI2O3	13.17	15.15	16.15	15.39	13.59	14.11	16.65	16.74	13.23	13.54	14.70	13.03	14.59	13.62
Fe2O3 (t)	6.02	3.27	5.58	12.20	13.05	3.01	12.98	5.42	3.02	3.31	4.08	1.53	5.55	0.61
MgO	1 35	0.66	1.91	5.81	3.13	0.70	4.51	1.46	0.33	0.78	0.83	0.48	1.61	0.17
CaO	2.88	2.85	4.33	6.46	6.80	1.85	4.58	4.03	0.59	1.77	2.02	2.69	3.84	1.90
Na2O	2.40	2.70	3.15	1.24	2.60	2.47	3.39	3.01	4.33	1.85	2.17	2.43	2.68	2.93
K2O	3.51	4.21	2.53	1.12	2.95	6.15	2.49	2.16	2.63	5.35	4.70	3.72	3.21	4.70
TiO2	0.73	0.36	0.57	0.99	2.10	0.36	2.07	0.61	0.26	0.46	0.24	0.15	0.67	0.07
P2O5	0.20	0.17	0.19	0.12	0.74	0.15	0.04	0.15	0.14	0.08	0.19	0.02	0.15	0.02
MnO	0.07	0.04	0.05	0.24	0.18	0.04	0.15	0.06	0.01	0.04	0.04	0.03	0.05	0.01
LOI	0.13	0.19	0.09	0.02	0.52	0.34	0.27	n.d	n.d	n.d	n.d	0.25	0.14	0.19
Total	98.47	99.28	99.80	101.80	99.14	97.88	99.31	98.85	101.04	100.03	99.70	98.87	98.92	99.38
FeO (t)	5 42	2.95	5.03	10.99	11.76	2.71	11.69	4.88	2.72	2.98	3.68	1.38	5.00	0.55
Mg#	31	29	40	49	32	32	41	35	18	32	29	38	36	36
$Na_2O + K_2O$	5.91	6.91	5.68	2.36	5.55	8.62	5.88	5.17	6.96	7.20	6.87	6.15	5.89	7.63
FeO/(FeO+MgO)	0.80	0.82	0.72	0.65	0.79	0.79	0.72	0.77	0.89	0.79	0.82	0.74	0.76	0.76
$Na_2O + K_2O$–CaO	3.03	4.06	1.35	−4.10	−1.25	6.77	1.30	1.14	6.37	5.43	4.85	3.46	2.05	5.73
Cs	0.118	0.167	0.016	2.620	0.233	0.120	0.156	0.232	0.045	0.163	0.230	0.098	0.074	0.316
Rb	126.4	190.5	54.6	59.9	97.0	285.6	27.7	94.4	42.7	139.4	189.8	82.8	83.6	194.2
Ba	661	487	571	550	1,295	445	1,676	681	690	869	626	817	899	645
Sr	149	118	176	256	324	94	586	289	29	122	96	162	144	184
Pb	15.9	17.3	18.2	14.0	17.1	21.9	18.2	15.9	8.4	34.6	29.2	24.3	15.8	24.2
Th	1.9	2.2	1.8	10.2	9.5	33.1	24.2	23.4	38.9	43.2	54.3	8.4	3.7	2.0
U	0.84	0.57	0.70	1.24	0.94	1.13	0.41	2.07	5.48	1.61	2.39	0.71	0.52	0.36
Zr	192.8	113.4	100.7	183.1	113.7	136.3	125.3	255.4	250.0	251.3	256.2	106.4	126.7	105.8
Ta	0.57	0.48	0.37	0.78	1.77	0.35	0.98	0.58	0.31	0.59	0.71	0.14	0.53	1.13
Y	24.0	29.0	10.0	40.0	52.0	17.0	30.0	25.5	54.7	34.5	55.7	2.5	2.5	1.7
Nb	18.76	14.34	11.87	11.06	31.37	10.58	24.29	9.18	11.22	13.46	19.70	1.95	11.27	32.26
Sc	14.4	8.7	11.2	40.9	32.1	7.7	23.3	11.0	13.0	17.0	9.0	5.5	16.1	30.6
Cr	16.7	7.6	21.0	56.0	20.9	5.1	174.4	7.0	7.0	15.0	15.0	5.2	19.1	154.3
Ni	12.07	3.83	16.39	68.10	18.80	9.24	81.58	28.00	14.00	11.00	11.00	2.67	13.86	76.81
Co	11.92	5.70	12.08	41.44	29.74	5.23	31.64	9.00	11.00	3 41	21.00	2.96	12.11	26.60
V	68.7	29.9	115.5	234.6	296.3	31.1	373.5	54.0	5.0	33.0	29.0	5.2	75.7	189.3

Table 1 continued

Sample	Charnoenderbites													
	TK54-1	TK54-2	TK74-1	TK 73-8	TK38-1	TK28-1	TK33-3	KR1-3	KR3-1	KR24-1	KR11-1	TK 36-2	TK 21	TK 58-2
Ga	17.2	16.9	18.4	15.8	19.5	15.3	21.2	21.0	16.0	16.0	20.0	10.6	17.6	22.6
Zn	59.73	23.54	85.93	98.57	132.37	20.86	76.10	64.00	19.00	38.00	39.00	11.52	68.91	156.92
Cu	25	6	10	57	30	8	66	31	n.d	n.d	n.d	5	24	36
La	40.0	40.0	29.0	30.0	119.0	57.0	75.0	87.3	82.3	86.4	98.5	33.6	58.5	29.1
Ce	72.0	72.0	53.0	59.0	245.0	104.0	117.0	153.4	157.5	158.3	192.8	43.2	93.2	36.8
Pr	7.8	7.6	6.1	6.8	28.0	11.0	9.9	15.7	17.8	16.7	21.4	4.1	9.3	3.5
Nd	29.0	28.0	23.0	26.0	102.0	38.0	34.0	50.7	61.2	54.6	74.0	12.9	32.3	9.6
Sm	5.20	5.20	5.00	5.90	18.00	6.70	5.50	8.24	13.61	9.51	15.09	1.68	4.09	1.09
Eu	1.40	1.30	1.50	1.40	3.10	1.20	2.20	1.44	1.11	1.28	1.34	2.06	1.71	0.88
Gd	4.60	5.40	4.30	6.40	15.00	5.60	5.70	5.83	11.87	6.62	12.41	0.96	2.46	0.65
Tb	0.79	b.d.l	0.63	1.20	2.20	0.78	0.94	0.82	1.93	0.94	1.87	0.10	0.21	0.07
Dy	4.40	5.80	2.30	7.10	11.00	3.80	5.30	4.61	11.34	5.89	10.65	0.50	0.77	0.33
Ho	0.91	1.10	0.40	1.50	2.00	0.64	1.00	0.90	2.10	1.28	2.00	0.10	0.10	0.06
Er	2.50	2.70	1.10	4.60	5.40	2.00	3.20	2.57	5.50	3.82	5.26	0.32	0.26	0.20
Tm	0.34	0.38	0.15	0.70	0.83	0.00	0.48	0.40	0.76	0.58	0.71	0.06	0.04	0.03
Yb	2.20	2.10	1.10	4.80	5.00	3.10	3.20	2.80	4.83	3.97	4.42	0.46	0.28	0.22
Lu	0.33	0.29	0.18	0.72	0.72	0.41	0.48	0.41	0.67	0.59	0.60	0.09	0.06	0.04
Eu/Eu*	0.87	0.75	0.99	0.70	0.58	0.60	1.20	0.64	0.27	0.49	0.30	4.96	1.65	3.19
K	29,138	34,948	21,002	9,297	24,489	51,053	20,670	17,931	21,832	44,412	39,016	30,881	26,647	39,016
Ti	4,350	2,145	3,397	5,899	12,514	2,145	12,335	3,635	1,549	2,741	1,430	894	3,993	417
P	873	742	829	524	3,230	655	175	655	611	349	829	87	655	87
Sr/Y	6.21	4.08	17.56	6.39	6.24	5.54	19.54	11.34	0.52	3.55	1.73	64.48	56.92	105.05
Th/Yb	0.87	1.07	1.65	2.12	1.90	10.67	7.57	8.39	8.06	10.88	12.28	18.29	12.98	9.05
Ta/Yb	0.26	0.23	0.34	0.16	0.35	0.11	0.31	0.21	0.06	0.15	0.16	0.29	1.89	5.13
Nb/Y	0.78	0.49	1.19	0.28	0.60	0.62	0.81	0.36	0.21	0.39	0.35	0.78	4.46	18.44
Y + Nb	42.76	43.34	21.87	51.06	83.37	27.58	54.29	34.64	65.89	47.91	75.43	4.46	13.79	34.01
Nb/La_{PM}	0.45	0.35	0.39	0.36	0.25	0.18	0.31	0.10	0.13	0.15	0.19	0.06	0.19	1.07
Zr/Nd_{PM}	0.80	0.49	0.53	0.85	0.13	0.43	0.45	0.61	0.49	0.56	0.42	1.00	0.47	1.33
La/Yb_{CN}	12.35	12.94	17.91	4.25	16.17	12.49	15.92	21.21	11.58	14.76	15.13	49.80	140.47	89.33
Tb/Yb_{CN}	1.60	0.00	2.55	1.11	1.96	1.12	1.31	1.30	1.79	1.05	1.88	0.95	3.26	1.35

LOI Loss on ignition. Mg# = 100Mg2*/(Mg2*+Fetot2*). $Eu/Eu^* = Eu_{CN}/(Gd_{CN}+Sm_{CN})/2$. $Nb/La_{PM} = (Nb/0.713)/(La/0.687)$. $Zr/Nd_{PM} = (Zr/11.20)/(Nd/1.354)$. $La/Yb_{CN} = (La/0.687)/(Yb/0.161)$. $Tb/Yb_{CN} = (Tb/0.0361)/(Yb/0.161)$; *n.d* not determined, *b.d.l* below detection limit

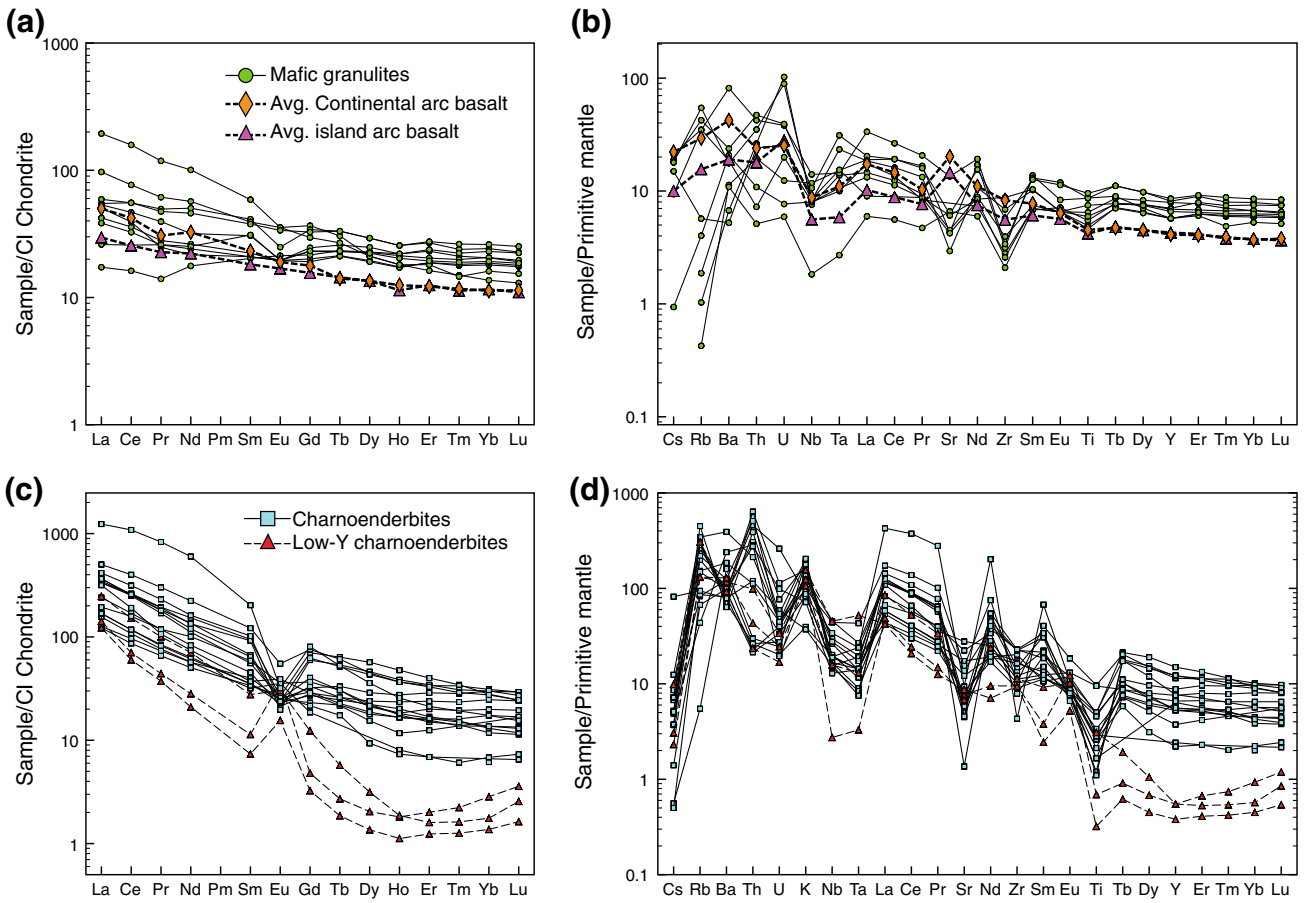

Fig. 5 **a** REE plot of mafic granulites normalized to C1 chondrite (McDonough and Sun 1995); **b** trace element plot of mafic granulites normalized to primitive mantle (Sun and McDonough 1989). In **a** and **b** average, REE and trace element values of continental and island arc basalts (Keleman et al. Kelemen et al. 2003) are plotted to compare with the analyzed data. **c** REE plot of charnoenderbites normalized to C1 chondrite (McDonough and Sun 1995); **d** trace element plot of charnoenderbites normalized to primitive mantle (Sun and McDonough 1989)

average 31 ppm), resulting in very low Sr/*Y* ratios (0.19–10.92, average 3.85). Nb contents vary from 1.31 to 10.0 ppm (average 6.21 ppm). The high *Y* contents result in a low Nb/*Y* ratio (0.04–0.23), which attest to their subalkaline affinity. This fact is also prominent in the TAS diagram (Fig. 3a). The mafic granulites show moderate Th/Yb (0.12–1.38) and Ta/Yb (0.12–0.30) ratios.

On the chondrite-normalized (normalizing values after McDonough and Sun 1995) rare earth element (REE) diagram (Fig. 5a), the mafic granulites display coherent REE patterns characterized by relative enrichment in LREE and nearly flat HREE pattern as indicated by La/Yb_{CN} of 0.75–6.01 (average 2.46) and Tb/Yb_{CN} of 1.01–1.66 (average 1.25). CN refers to the respective chondrite-normalized values. The samples show very minor negative or no Eu anomalies (Eu/Eu* = 0.664–1.044, mean 0.88). These patterns are very similar to the patterns shown by the average values of continental and island arc basalts (Fig. 5a) as compiled by Kelemen et al. (2003).

On the primitive mantle-normalized (normalizing values after Sun and McDonough 1989) extended trace element diagram (Fig. 5b), the mafic granulites display negative anomalies of Nb (Nb/La_{PM} = 0.31–0.94, mean 0.54) and negative to slightly positive anomalies of Zr (Zr/Nd_{PM} = 0.18–1.03, mean 0.43) relative to elements of similar degree of incompatibility. PM represents respective primitive-normalized values. Except for two, the samples show a slightly negative Ta anomaly (Fig. 5b). Ti shows minor negative anomalies. Like the chondrite-normalized REE patterns, the primitive mantle-normalized trace element patterns of the mafic granulites from the Ongole domain are also similar (Fig. 5b) to that of the average values of continental and island arc basalts (Kelemen et al. 2003).

Charnoenderbites Major and trace element compositions of the charnoenderbites from the Ongole domain are presented in Table 1. The samples have SiO_2 = 52.2–75.2 wt% (aver-

age 66.1 wt%), TiO_2 = 0.1–2.1 wt%, total Fe_2O_3 = 0.61–13.1 wt%, MgO = 0.2–5.8 wt%, Al_2O_3 = 13.0–16.7 wt%, CaO = 1.8–6.0 wt% and $Na_2O + K_2O$ = 2.4–7.9 wt%. Mg# = 29.8–40.8. Major and trace element variation diagrams show that SiO_2 is negatively correlated with MgO, total Fe_2O_3, CaO, Ni and Cr and positively correlated with K_2O (Fig. 4).

Similar to the mafic granulites, the charnoenderbites have variable but low Sr contents (28–586 ppm, average 211 ppm) and high *Y* contents (10–68 ppm, average 33 ppm) resulting in low Sr/*Y* ratios (2.1–33.0, average 9.2). There are three samples (TK21, TK36-2 and TK58-2) that have low Sr contents (143–183 ppm) and very low *Y* contents (1.8–2.5 ppm) resulting in high Sr/*Y* ratios (57–105), which is very different from the rest of the samples. Henceforth, these three samples will be referred to as low *Y* charnoenderbites. Nb contents (11–32 ppm) and the high *Y* contents of the remaining samples result in low Nb/*Y* ratio (0.2–1.2, average 0.6) conforming the subalkaline nature of these rocks, which is also evident from the TAS diagram (Fig. 3a). The charnoenderbites show variable Th/Yb (1.1–25.5) and high Ta/Yb (0.1–0.6) ratios, while the low *Y* charnoenderbites have similar Th/Yb ratios (9.1–18.3) but higher Ta/Yb ratios (0.3–5.1) than the other charnoenderbites.

On the chondrite-normalized rare earth element diagram (McDonough and Sun 1995; Fig. 5c), the charnoenderbites display highly fractionated REE patterns characterized by the relative enrichment in the LREE compared to the HREE as indicated by the high ratios of La/Yb_{CN} = 4.2–71.1 (average 19.1). The HREE patterns are rather flat as indicated by the low ratios of Tb/Yb_{CN} = 1.1–3.0 (average 1.6). They are characterized by negative to absent Eu anomalies (Eu/Eu* = 0.25–0.99) with the exception of two samples with slightly positive Eu anomalies (1.2 and 1.5). The low *Y* charnoenderbites (Fig. 5c) are characterized by highly enriched LREE compared with HREE (La/Yb_{CN} = 49.8–140.5), distinct concave-up trends in the HREE and positive Eu anomalies (Eu/Eu* = 1.65–4.96). Overall, the MREE and HREE in the low *Y* charnoenderbites are highly depleted compared with the other charnoenderbites (Fig. 5c).

On the extended trace element plot (Fig. 5d), the charnoenderbites display relative enrichment of the fluid mobile large ion lithophile elements (LILE, except Cs) and are characterized by large negative Nb–Ta anomalies (Nb/La_{PM} = 0.04–0.45, mean 0.26) and negative Zr anomalies (Zr/Nd_{pm} = 0.02–1.05, mean 0.48). They also display negative Ti and Sr anomalies. The low *Y* charnoenderbites show negative to slightly positive Nb–Ta anomalies (Nb/La_{pm} = 0.06–1.07).

U–Pb zircon geochronology

A total of six samples were selected for laser ablation inductively coupled plasma mass spectrometry (LA-ICP-MS) U–Pb spot analyses on separate zircon grains. Out of these, five separates derive from charnoenderbites (TK4B2, TK21, TK28-1, TK39-3 and TK39-4) of different parts of the Ongole domain. In addition, zircon grains from one orthogneiss (TK66-1) of the Vinjamuru domain were analyzed. The results of the U–Pb isotopic analyses are presented in Table 3 (electronic appendix). Analyses only with a degree of concordance of 100 ± 2 % have been considered for concordant age calculation.

TK4b2

The enderbite (TK4B2) from Kondapalle preserves a peak assemblage of Grt-Opx-Pl-Kfs-Qz. The zircon grains are prismatic and euhedral to subhedral and range from 150 to 300 μm in length. CL images reveal weakly luminescent well-developed oscillatory-zoned cores for most zircon grains, surrounded by broad, unzoned overgrowths having slightly higher luminescence (Fig. 6a). The oscillatory-zoned cores are sometimes partly corroded, over which broad unzoned rims have grown (Fig. 6a). A few grains exhibit a narrow, unzoned, highly luminescent intermediate part surrounding the partly corroded zoned cores (Fig. 6a). In most of the grains, these intermediate zones are too narrow to be analyzed with the LA-ICP-MS. The oscillatory-zoned cores have varying *U* contents (461–2,787), while the rims have lower *U* contents (262–1,144 ppm).

A total of 30 spots on 11 zircon grains were analyzed. The oscillatory-zoned core domains of the zircon grains yield a Paleoproterozoic concordia age of 1,717.0 ± 13.0 Ma, defined by nine concordant analyses (Fig. 7a). The unzoned broad overgrowths around the core domains define a late Paleoproterozoic concordia age of 1,626.4 ± 9.1 Ma from 15 concordant analyses (Fig. 7a), which is ca. 90 Ma younger than the oscillatory-zoned core domains. A single grain (Fig. 6a) in which the highly luminescent intermediate zone is broad enough to be analyzed yielded a Pb–Pb age of 1,652 ± 48 Ma, which is slightly older than the concordant age obtained from the rims. However, within error, it gives the same age as that of the broad rims.

TK21

The charnockite (TK21) from the south of the Guntur region preserves a peak mineral assemblage of Grt-Opx-Pl-Kfs-Qz. The zircon grains are prismatic and euhedral to

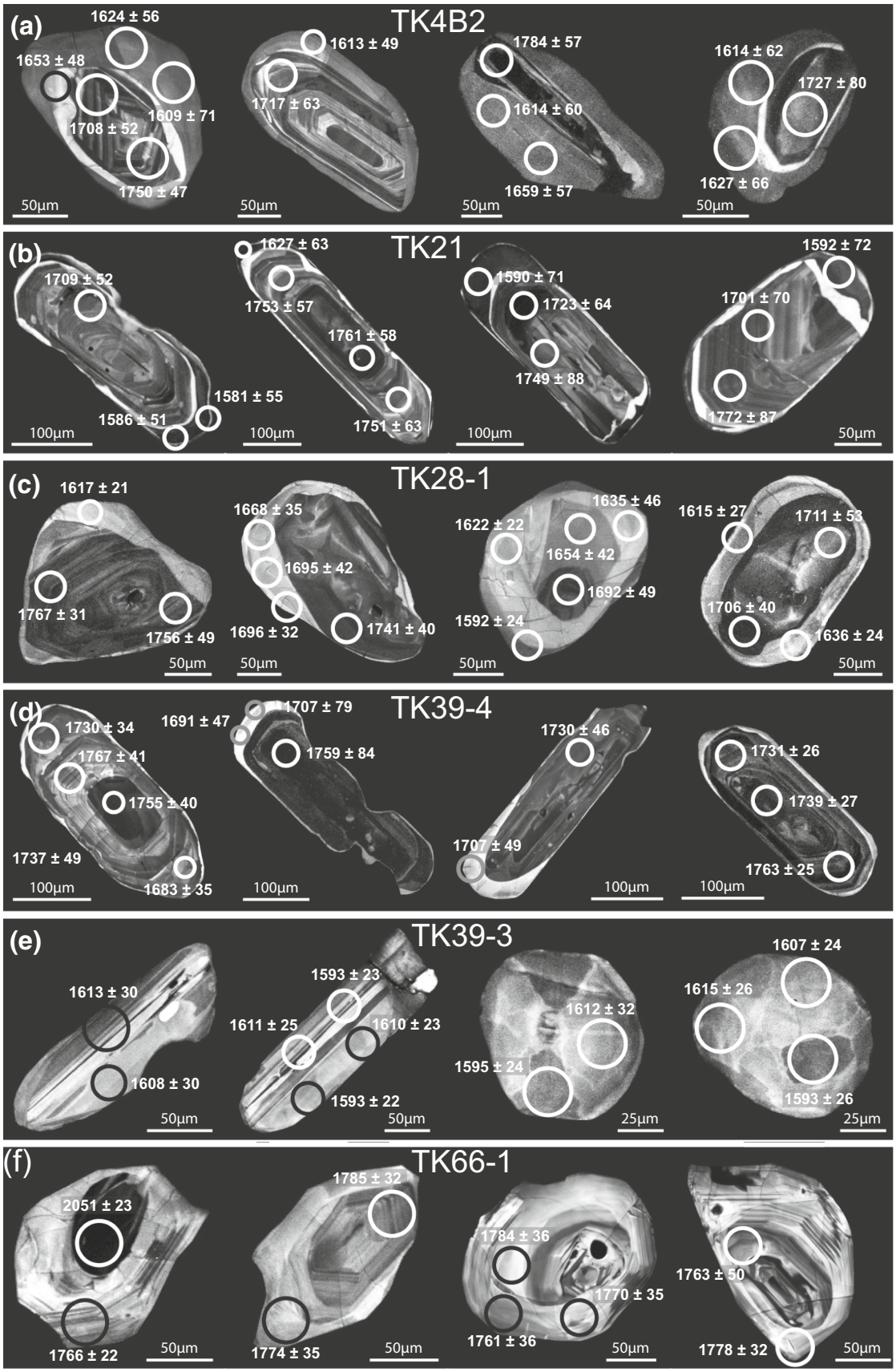
(a)
TK4B2
1624 ± 56
1653 ± 48
1609 ± 71
1708 ± 52
1750 ± 47
1613 ± 49
1717 ± 63
1784 ± 57
1614 ± 60
1659 ± 57
1614 ± 62
1727 ± 80
1627 ± 66
50µm
(b)
TK21
1709 ± 52
1581 ± 55
1586 ± 51
1627 ± 63
1753 ± 57
1761 ± 58
1751 ± 63
1590 ± 71
1723 ± 64
1749 ± 88
1592 ± 72
1701 ± 70
1772 ± 87
100µm
50µm
(c)
TK28-1
1617 ± 21
1767 ± 31
1756 ± 49
1668 ± 35
1695 ± 42
1696 ± 32
1741 ± 40
1622 ± 22
1635 ± 46
1654 ± 42
1692 ± 49
1592 ± 24
1615 ± 27
1711 ± 53
1706 ± 40
1636 ± 24
50µm
(d)
TK39-4
1730 ± 34
1767 ± 41
1755 ± 40
1737 ± 49
1683 ± 35
1691 ± 47
1707 ± 79
1759 ± 84
1730 ± 46
1707 ± 49
1731 ± 26
1739 ± 27
1763 ± 25
100µm
(e)
TK39-3
1613 ± 30
1608 ± 30
1593 ± 23
1611 ± 25
1610 ± 23
1593 ± 22
1612 ± 32
1595 ± 24
1607 ± 24
1615 ± 26
1593 ± 26
50µm
25µm
(f)
TK66-1
2051 ± 23
1766 ± 22
1785 ± 32
1774 ± 35
1784 ± 36
1770 ± 35
1761 ± 36
1763 ± 50
1778 ± 32
50µm

◀**Fig. 6** CL images of selected zircon grains from the samples of the Ongole domain **a**–**e** and the adjoining Vinjamuru domain **f**. Circles mark the position of the laser spot (*scaled to size*). Ages are presented as $^{207}Pb/^{206}Pb$ ages (in Ma) with 2σ error. **a** Well-developed oscillatory-zoned cores surrounded by broad unzoned rims. Sometimes a bright zone in between the core and the rims is present; **b** elongated zircon grains with well-developed oscillatory-zoned cores surrounded by two consecutive bright and dark narrow rims; **c** anhedral zircon grains with resorbed cores (sometimes oscillatory-zoned) surrounded by broad and bright rims; **d** prismatic zircon grains having dark oscillatory-zoned cores surrounded by narrow-to-broad bright rims. **e** Elongated and rounded zircon grains. The elongated grains show resorbed zoned cores and unzoned rims having variable thickness. The rounded grains show sector zoning. **f** anhedral zircon grains with preserved oscillatory-zoned xenocrystic cores. The cores are partly resorbed and overgrown by oscillatory-zoned mantles that truncate the zoning pattern of the cores

subhedral, mostly ranging from 200 to 350 μm in length, with a few larger grains up to 450 μm. CL images reveal moderately luminescent well-developed oscillatory zoning for most zircon grains (Fig. 6b). Most of the zircon grains show two consecutive narrow unstructured overgrowths with some resorption of the marginal parts of the oscillatory-zoned grains (Fig. 6b). A highly luminescent inner zone around the core is normally very narrow (<20 μm) making it difficult for precise measurement with the LA-ICP-MS. The weakly luminescent outer overgrowths are normally very narrow along the length, but are wider (up to 50 μm) around the corner, where they could be analyzed comfortably (Fig. 6b). The cores and the rims have similar *U* contents (230–1,017 ppm).

A total of 35 spots on 13 grains were analyzed. The oscillatory-zoned core domains of the zircon grains yield a Paleoproterozoic concordia age of 1,743.0 ± 10.0 Ma, defined by 13 concordant analyses (Fig. 7c). The weakly luminescent, zoned outer overgrowths define a very late Paleoproterozoic concordia age of 1,600.5 ± 9.8 Ma from 13 concordant analyses (Fig. 7d). This age is ca. 143 Ma younger than the age obtained from the core.

TK28-1

The charnockite (TK28-1) from Kondapalle preserves a peak assemblage of Grt-Opx-Kfs-Pl-Qz. The zircon grains are mostly subhedral to anhedral. Some are rounded to elliptical. They are in the size range of 150–300 μm in length. CL images reveal very weakly luminescent, oscillatory or sector zoning in the core domains of most zircon grains (Fig. 6c). Due to the very low luminescence, the very fine oscillatory zoning in the cores is not very prominent in most of the grains. The majority of the cores exhibits resorption along their margins and is overgrown by narrow-to-broad unzoned luminescent rims (Fig. 6c). The dark cores have very high *U* contents (1,111–4,277 ppm), while the brighter rims have lower contents (188–969 ppm).

A total of 44 spots on 12 zircon grains were analyzed. The weakly luminescent oscillatory-zoned core domains yield a concordia age of 1,719.6 ± 9.5 Ma, defined by 11 concordant analyses (Fig. 7e). The luminescent narrow-to-broad rims display two different age populations. The rims of most of the grains define a concordia age of 1,687.7 ± 8.3 Ma from 13 concordant analyses (Fig. 7f). The rims of the other grains define an upper intercept age of 1,620 ± 9 Ma from 16 analyses (Fig. 7g). Among them, seven concordant analyses yield a concordia age of 1,612.1 ± 14.0 Ma from seven concordant analyses (Fig. 7h), similar to that of the upper intercept age. However, the rims with two different ages could not be separated petrographically under CL images or chemically from *U* contents.

TK39-4

The charnockite (TK39-4) from the north of the Kondapalle region preserves a peak assemblage of Grt-Opx-Kfs-Pl-Qz. The zircon grains are prismatic and euhedral to subhedral and mostly range from 200 to 350 μm in length. CL images reveal weakly luminescent, well-developed oscillatory zoning for most zircon grains (Fig. 6d). Some grains exhibit a slightly zoned or unzoned dark mantle around the oscillatory-zoned core. Very often narrow (<10 μm), moderate to highly luminescent, unzoned rims surround the grains (Fig. 6d). In only a few grains, these rims are broader, where they could be analyzed (Fig. 6d). The *U* content in the cores varies widely from 329 to 3,437 ppm, while the rims have low *U* contents from 179 to 1,074 ppm.

A total of 42 spots on 12 zircon grains were analyzed. The weakly luminescent oscillatory-zoned domains yield a concordia age of 1,745.8 ± 8.2 Ma, defined by 14 concordant analyses (Fig. 7i). The highly luminescent rims define a concordia age of 1,715.6 ± 8.4 Ma from 11 concordant analyses (Fig. 7j). Four discordant analyses from the rims yield Pb–Pb ages from 1,683 ± 53 to 1,644 ± 48 Ma (Table 3 in electronic appendix).

TK39-3

The fine-grained enderbite (TK39-3) is a sheared rock with the mineral assemblage of Grt-Pl-Kfs-Qz intruding into the charnockite (TK39-4). The zircon grains show contrasting morphological features. Some zircon grains are prismatic and euhedral to subhedral, ranging from 100 to 250 μm in length (Fig. 6e), while others are spherical to ellipsoidal ranging from 50 to 100 μm in diameter (Fig. 6e). CL

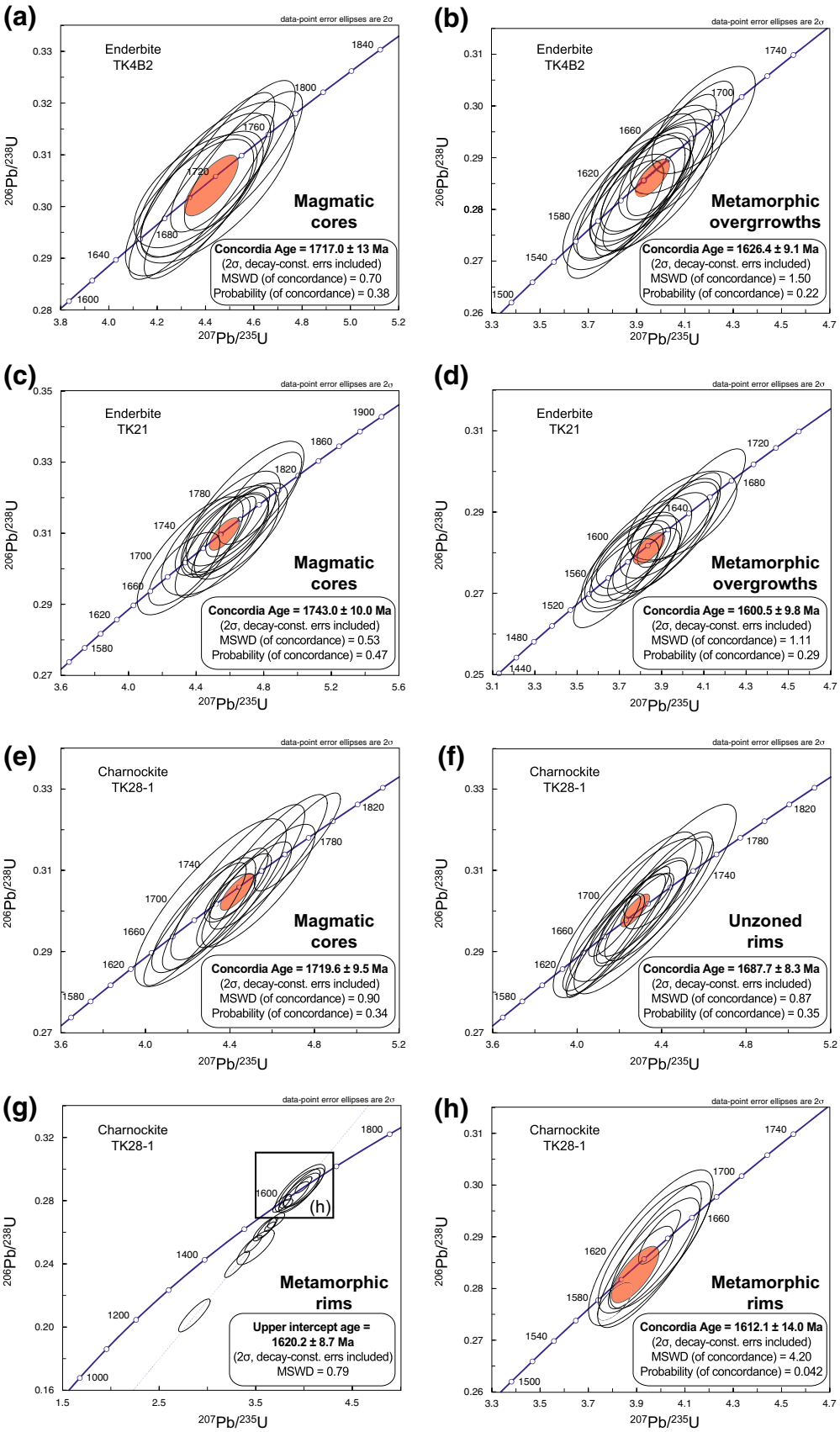
(a)
Enderbite
TK4B2
Magmatic cores
Concordia Age = 1717.0 ± 13 Ma
(2σ, decay-const. errs included)
MSWD (of concordance) = 0.70
Probability (of concordance) = 0.38
(b)
Enderbite
TK4B2
Metamorphic overgrrowths
Concordia Age = 1626.4 ± 9.1 Ma
(2σ, decay-const. errs included)
MSWD (of concordance) = 1.50
Probability (of concordance) = 0.22
(c)
Enderbite
TK21
Magmatic cores
Concordia Age = 1743.0 ± 10.0 Ma
(2σ, decay-const. errs included)
MSWD (of concordance) = 0.53
Probability (of concordance) = 0.47
(d)
Enderbite
TK21
Metamorphic overgrowths
Concordia Age = 1600.5 ± 9.8 Ma
(2σ, decay-const. errs included)
MSWD (of concordance) = 1.11
Probability (of concordance) = 0.29
(e)
Charnockite
TK28-1
Magmatic cores
Concordia Age = 1719.6 ± 9.5 Ma
(2σ, decay-const. errs included)
MSWD (of concordance) = 0.90
Probability (of concordance) = 0.34
(f)
Charnockite
TK28-1
Unzoned rims
Concordia Age = 1687.7 ± 8.3 Ma
(2σ, decay-const. errs included)
MSWD (of concordance) = 0.87
Probability (of concordance) = 0.35
(g)
Charnockite
TK28-1
(h)
Metamorphic rims
Upper intercept age =
1620.2 ± 8.7 Ma
(2σ, decay-const. errs included)
MSWD = 0.79
(h)
Charnockite
TK28-1
Metamorphic rims
Concordia Age = 1612.1 ± 14.0 Ma
(2σ, decay-const. errs included)
MSWD (of concordance) = 4.20
Probability (of concordance) = 0.042
data-point error ellipses are 2σ
206Pb/238U
207Pb/235U

◀ **Fig. 7** U–Pb concordia diagrams for the charnoenderbites of the Ongole domain and a orthogneiss from the adjoining Vinjamuru domain. Concordia ages are given with 2σ standard uncertainties

images reveal highly luminescent growth banding and sector zoning for the elongated zircon grains and moderately luminescent sector zoning for the spherical to ellipsoidal grains. Many elongated grains show different degrees of resorption of the zoned domains and development of unzoned domains (Fig. 6e). The spherical to ellipsoidal grains do not display such features. The zoned cores and the unzoned domains have similar *U* contents of 119–450 ppm.

A total of 36 spots on 14 zircon grains were analyzed. The zoned domains of the elongated zircon grains yield a concordia age of 1,602.6 ± 7.2 Ma, defined by 12 concordant analyses (Fig. 7k). However, the concordia diagram clearly indicates that there is a spread of ages. The resorbed and recrystallized unzoned domains of the elongated grains and the sector-zoned, spherical to ellipsoidal grains define a concordia age of 1,602.1 ± 4.5 Ma from 14 concordant analyses (Fig. 7l), the same age as that from the zoned cores.

TK66-1

The amphibolite facies orthogneiss (TK66-1) of the Vinjamuru domain (near Chundi village) preserves a peak mineral assemblage of Qz-Pl-Kfs-Bt. The zircon grains are subhedral to anhedral, ranging from 100 to 200 μm in length. CL images reveal that most of the zircon grains have a distinct core and mantle. Some grains have weakly luminescent (very dark) spherical to ellipsoidal cores, while the others preserve moderately luminescent, well-preserved oscillatory-zoned cores (Fig. 6f). The zoned cores are separated from their rims by surfaces (sometimes geometrically irregular) that truncate the internal zoning pattern (Fig. 6f). The broad rims are moderate to highly luminescent and show well-preserved oscillatory growth zoning. The discontinuities between the core and the rims indicate deep resorption of the early zircon phase, and locally, they reveal that the new zircon growth occurred in a different crystallographic orientation than the substrate zircon. Both cores and the rims have very low *U* contents (114–263 ppm).

A total of 41 spots on 17 zircon grains were analyzed for U–Pb isotopes. The spherical to ellipsoidal dark cores yielded a range of Pb–Pb spot ages from 2,436 ± 19 Ma to 1,869 ± 41 Ma (Table 3 in electronic appendix). Several of these cores were completely metamict, and no age could be obtained. The oscillatory-zoned xenocrystic cores yield a concordia age of 1,777.9 ± 6.1 Ma, defined by 12 concordant analyses (Fig. 7m). The more luminescent well-preserved oscillatory-zoned rims also yield the same concordia age of 1,777.6 ± 6.4 Ma, defined by nine concordant analyses (Fig. 7n).

Discussion

Timing of formation and metamorphism of the Ongole domain

The oscillatory zoning in the core domains of the zircon grains of the enderbitic gneiss (TK4B2) suggests that they represent parts of the magmatically grown zircon crystals. The zircon grains were partly resorbed before being overgrown by broad unzoned rims. The Paleoproterozoic age of ca. 1,720 Ma obtained from the core domains is interpreted to be the age of intrusion of the granodioritic precursor of the enderbite (Figs. 6a,7a; Table 2). The late Paleoproterozoic age of ca. 1,630 Ma obtained from the broad, unzoned rims is interpreted to be the age of granulite-facies peak metamorphism (Figs. 6a,7b; Table 2).

The large, prismatic, well-developed, oscillatory-zoned zircon grains from the enderbitic gneiss (TK21) indicate that they are magmatic zircon grains. Therefore, the Paleoproterozoic age of ca. 1,740 Ma obtained from the oscillatory-zoned domains of the zircon grains (Figs. 6b, 7c; Table 2) reflects the age of the magmatic intrusion. The late Paleoproterozoic age of ca. 1,600 Ma obtained from the unzoned, weakly luminescent outer rims indicates the age of peak metamorphism (Figs. 6b, 7d; Table 2). The highly luminescent narrow rims between the zoned cores and the unzoned rims in both the samples (TK4B2 and TK21; Fig. 6a, b) could not be measured properly with the LA-ICPMS. Due to the lack of data, the exact timing of the formation and hence the geological significance could not be resolved. However, petrographically, it seems that these bright rims formed by resorption and subsequent recrystallization of the oscillatory-zoned zircon cores prior to the growth of the broad rims.

The Paleoproterozoic age of ca. 1,720 Ma obtained from the large, oscillatory or sector-zoned zircon grains in the charnockite (TK28-1) is interpreted as the age of intrusion of the granitic protolith of the charnockite (Figs. 6c, 7e; Table 2). The late Paleoproterozoic age of ca. 1,610 Ma obtained from the rims of some zircon grains (Figs. 6c, 7h; Table 2) is consistent with the ages obtained from the metamorphic rims and overgrowths in zircon of other charnoenderbites, representing the age of the peak metamorphism. The brightly luminescent rims from the other zircon grains yielding a Paleoproterozoic age of ca. 1,690 Ma are not easy to interpret (Figs. 6c, 7f). Still there is no strong evidence from other rocks to assign this age as the timing of another tectonometamorphic event in the region. However, Kovach et al. (2001) reported concordant U–Pb

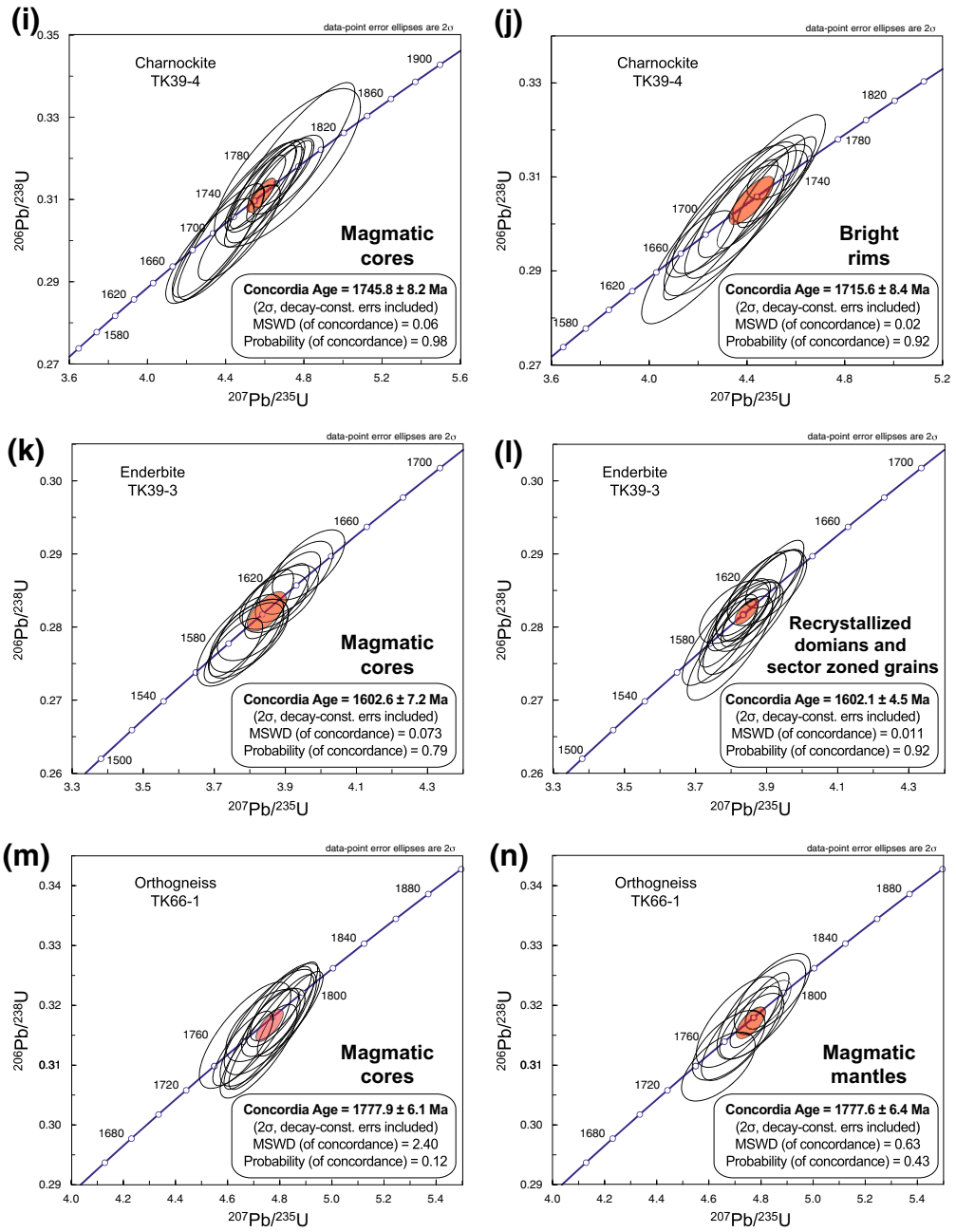

Fig. 7 continued

monazite ages of ca. 1,670 Ma and interpreted that as the age of the syn-kinematic formation of the coarse-grained leucosome network in the charnoenderbites, but the geological interpretation is not unambiguous.

Similar to other charnoenderbites, the Paleoproterozoic age of ca. 1,750 Ma obtained from the oscillatory-zoned large zircon grains in the charnockite TK39-4 represents the magmatic intrusion age (Figs. 6d, 7i; Table 2). The implications of the Paleoproterozoic age of ca. 1,715 Ma, obtained from the highly luminescent unzoned or weakly zoned overgrowths (Figs. 6d, 7j; Table 2), are again not straightforward. Considering the lack of evidence from other rocks to correlate this age with any regional event, we interpret this age as a period of renewed zircon growth due to local fluid circulations during the last stage of magma crystallization.

The prismatic, euhedral zircon grains in the sheared enderbite (TK39-3) strongly argue for a magmatic origin. Consequently, the concordia age of ca. 1,600 Ma represents the age of intrusion of the precursor magma (Figs. 6e, 7k;

Table 2 Sample locations, descriptions of zircon textures under CL, corresponding U-Pb ages of zircon growth and geological interpretation of the age

Sample	Rock type	GPS coordinates	Zircon populations and textures under cathodoluminescence (CL)	Interpretation of zircon growth	Ages (Ma)	Geological interpretation
Ongole domain						
TK4B2	Enderbite	N 16° 36.374′	Two zircon populations are distinguished			
		E 80° 31.982′	(Pop1) Subhedral zircon grains (up to 300 μm) having weakly luminescent well-developed oscillatory-zoned cores (Fig. 7a)	(1) Magmatic	(1) Concordia age 1717 ± 13 (Fig. 8a)	(1) Magmatic protolith emplacement
			(Pop2) Broad, unzoned overgrowths around cores (occasionally resorbed) having slightly higher luminescence (Fig. 7a)	(2) Metamorphic	(2) Concordia age 1,626 ± 9 (Fig. 8b)	(2) Granulite-facies metamorphism
TK21	Enderbite	N 16° 11.581′	Two zircon populations are identified			
		E 80° 15.816′	(Pop1) Elongated zircon grains (up to 350 μm) with moderately luminescent well-developed oscillatory-zoned cores (Fig. 7b)	(1) Magmatic	(1) Concordia age 1,743 ± 10 (Fig. 8c)	(1) Magmatic protolith emplacement
			(Pop2) Two consecutive narrow unstructured overgrowths; (2a) narrow highly luminescent inner zone; (2b) weakly luminescent outer zone (Fig. 7b)	(2a) Not known (2b) Metamorphic	(2a) Could not be measured (2b) Concordia age 1,601 ± 10(Fig. 8d)	(2b) Granulite-facies metamorphism
TK28-1	Charnockite	N 16°37.440′	Two zircon populations are identified			
		E 80°31.978′	(Pop1) Subhedral (up to 300 μm) weakly luminescent, oscillatory or sector-zoned cores (Fig. 7c)	(1) Magmatic	(1) Concordia age 1,720 ± 10 (Fig. 8e)	(1) Magmatic protolith emplacement
			(Pop2) Moderately luminescent narrow-to-broad unzoned overgrowths surrounding the zoned cores (Fig. 7c). Pop2 yields two concordia ages.	(2) Metamorphic	(2a) Concordia age 1,688 ± 8 (2b) Concordia age 1,612 ± 14 (Fig. 8f & h)	(2a) Interpretation no clear(2b) Granulite-facies metamorphism
TK39-4	Charnockite	N 16°40.545′	CL images reveal two zircon populations			
		E 80°34.253′	(Pop1) Prismatic zircon grains (up to 350 μm) having weakly luminescent well-developed oscillatory-zoned cores (Fig. 7d)	(1) Magmatic	(1) Concordia age 1,746 ± 8 (Fig. 8i)	(1) Magmatic protolith emplacement
			(Pop2) Highly luminescent narrow unzoned rims surrounding the zoned cores (Fig. 7d)	(2) Magmatic	(2) Concordia age 1,716 ± 8 (Fig. 8j)	(2) Crystallization from late-stage magmatic fluids
TK39-3	Enderbite	N 16°40.545′	Two zircon populations are distinguished			
		E 80°34.253′	(Pop1) Prismatic, euhedral zircon grains (up to 250 μm) with highly luminescent growth banding (Fig. 7e)	(1) Magmatic	(1) Concordia age 1,603 ± 7 (Fig. 8k)	(1) Magmatic protolith emplacement
			(Pop2) Unzoned or planar banded overgrowths that embay and truncate the early zoning. Pop2 zircon also forms anhedral grains showing patchy or sector zoning (Fig. 7e)	(2) Anatectic and metamorphic	(2) Concordia age 1,602 ± 5 (Fig. 8l)	(2) Granulite-facies metamorphism (Syn-metamorphic intrusion)
Vinjamuru domain						
TK66-1	Orthogneiss	N 15°09.809′	Three zircon populations are recognized in the subhedral zircon grains (up to 200 μm)			
		E 79°33.562′	(Pop1) Weakly luminescent rounded to ellipsoidal cores (Fig. 7f)	(1) Inherited	(1) $^{207}Pb/^{206}Pb$ ages 2,436–1,869	(1) Magmatic or metamorphic event
			(Pop2) Oscillatory-zoned, moderately to weakly luminescent xenocrystic cores	(2) Magmatic	(2) Concordia age 1,778 ± 6 (Fig. 8m)	(2) Magmatic protolith emplacement
			(Pop3) Broad, moderately to highly luminescent, oscillatory-zoned overgrowths that may truncate the core zoning but also form conformable to the cores (Fig. 7f)	(3) Magmatic	(3) Concordia age 1,778 ± 6 (Fig. 8n)	(3) Resorption and overgrowth during magmatic activity

Table 2). On the other hand, the unzoned, recrystallized domains of the elongated grains and the ellipsoidal sector-zoned zircon indicate a metamorphic origin (Figs. 6e, 7l; Table 2). Therefore, the concordia age of ca. 1,600 Ma obtained from these grains is interpreted to be the age of peak metamorphism, consistent with the metamorphic ages obtained from the other charnoenderbites. Magmatic zircon grains having the same age as the metamorphic overgrowths have not been encountered before. The most plausible interpretation is that the precursor rock intruded during ongoing metamorphism and deformation, indicating that this enderbite is a syn-metamorphic intrusion. The intrusive relationship of the fine-grained sheared enderbite into the older (ca. 1,750 Ma) coarse-grained charnockite (TK39-4) further conforms with this interpretation.

The dark, spherical to ellipsoidal core domains of zircon grains of the orthogneiss (TK66-1), from the adjoining Vinjamuru domain, showing a range of Paleoproterozoic ages from ca. 2,430–1,870 Ma represent inherited cores, which were incorporated into the magma from the surrounding country rocks during intrusion or melting of the source rocks (Fig. 6f; Table 2). The oscillatory-zoned outer parts of the cores clearly indicate that they are magmatically grown zircon grains. These grains were resorbed to different extents before the crystallization of a broad oscillatory-zoned mantle that is also of magmatic origin. The zoned cores as well as the zoned mantles yielding the same concordia age (ca. 1,780 Ma; Fig. 7m, n; Table 2) imply that they were formed during the same magmatic event.

The zircon U–Pb geochronological data from the current study (Table 2) constrain the timing of the intrusion of the precursor magmas of charnoenderbites, the dominant rocks of the Ongole domain and the timing of the metamorphism. From the four charnoenderbite samples, the concordant ages from the oscillatory-zoned magmatic cores range from ca. 1,750 to 1,710 Ma. We interpret this age span (ca. 40 Ma) as the duration of widespread magmatic activity in the region. This implies that the crust formation of the Ongole domain was in the Paleoproterozoic. The ages from this study are in agreement with the age of emplacement (1.72–1.70 Ga) reported by Kovach et al. (2001) in a preliminary study.

The concordant ages from the unzoned metamorphic overgrowths, in three charnoenderbite samples, range from ca. 1,630 to 1,600 Ma, constraining the timing of the granulite-facies metamorphism in the Ongole domain. This age range is identical to the concordant metamorphic ages of ca. 1,625–1,600 Ma obtained from zircons of five metapelitic samples that occur as enclaves within these charnoenderbites (Sarkar et al. 2014). This age is interpreted to reflect the timing of UHT granulite-facies metamorphism and partial melting in the Ongole domain. Thus, the concordant metamorphic ages (ca. 1,630–1,600 Ma) from eight different rocks (three from this study and five from Sarkar et al. 2014) from different localities tightly constrain the timing and duration (ca. 30 Ma) of the UHT granulite-facies metamorphism and partial melting the Ongole domain. The age is further supported by in situ Th-U-total Pb dating of monazites from the same metapelites, where the monazite inclusions in garnet yield ages of ca. 1,610 Ma (Sarkar et al. 2014). Additionally, monazite dating of five different samples (three metapelites and three charnoenderbites) yielded a younger age of ca. 1,540 Ma, interpreted to be the age of a second metamorphic event that occurred 60–80 Ma after the first. Incidentally, this age was neither preserved in zircon grains from the metapelites (Sarkar et al. 2014), nor in zircon grains from the charnoenderbites of the present study.

The syn-metamorphic charnockite intrusion into older charnoenderbites sheds some more light on the causes for the UHT metamorphism. Sarkar and Schenk (2014) argued based on petrological and thermobarometric constrains that the first metamorphic event with UHT peak conditions (ca. 1,620 Ma) is characterized by an isobaric heating–cooling trajectory, which points toward a magmatic heat source for the metamorphism. The syn-metamorphic enderbitic intrusion most likely represents a fractionated melt from a bigger mafic intrusion that probably contributed heat for the UHT metamorphism.

Concordant magmatic ages of ca. 1,780 Ma from the oscillatory-zoned cores and mantles of the zircon grains from the orthogneiss of the Vinjamuru domain (TK66-1; Fig. 7m, n) clearly indicate the age of emplacement, which is slightly older but similar to the emplacement age of the charnoenderbites in the Ongole domain. The age is in agreement with zircon ages (ca. 1,790–1,770 Ma) from similar metamorphosed felsic rocks that show major and trace element chemistry of a volcanic arc granite (Ravikant et al. 2013).

Petrogenesis of the mafic granulites

As the ratio of two incompatible elements mostly remain unchanged during partial melting as well as fractional crystallization (Pearce and Peate 1995), the incompatible elements can be used as tracers for magmatic processes. The two important elements for tracing subduction zone processes are Nb and Ta as depletion of primitive arc magmas in Nb and Ta relative to Th and La is ubiquitous and has been ascribed to many processes (Kelemen et al. 2003). The primary reason for depletion is the preferential retention of Nb and Ta within mineral phases (e.g., rutile, ilmenite) in rocks of subduction zones (e.g., Pearce and Peate 1995). These minerals are either present as residual phases in the area of melt production and/or separated during fractional crystallization from the magma. Depletion in Zr indicates

that the neighboring LREE are relatively enriched compared to Zr, which is one of the most immobile elements. Nb and Ta depletions coupled with Ti and Zr depletions, like in the mafic granulites of the Ongole domain (Fig. 5b), are therefore a unique characteristic of melts generated in a magmatic arc.

The mafic granulites also display other trace element signatures that are typical of volcanic rocks erupting at modern day volcanic arcs. The rocks are characterized by LREE enrichment (Fig. 5a) and moderate depletion in HREE leading to Sr/*Y* ratios in the range of 0.19–10.92 (Fig. 8a) and La/Yb_{CN} ratios of 0.75–6.01 (Fig. 8b). These along with low TiO_2 (<0.2 wt%) contents (Pearce and Cann 1973) suggest that the mafic granulites are typical of calc-alkaline subduction-related magmas (e.g., oceanic island arc or continental arc). The mafic granulite suite also falls mainly in the island field of the La-Sm-Th-Yb-Nb log-transformed discrimination diagram (Agrawal et al. 2008; Fig. 8d).

As continental rocks are highly differentiated and enriched in incompatible elements compared to the upper mantle (e.g., Rudnick 1995), the ratios of incompatible elements are also useful in investigating the role of crustal contamination in mantle-derived melts. Incompatible trace element ratios such as Th/Yb and Ta/Yb are used to investigate the role of the subcontinental lithosphere in magma genesis at oceanic arcs and active continental margins (Pearce 1983). The rocks formed at active continental margins have higher Th/Yb (1.0–10.0) and Ta/Yb (0.1–1.0) ratios than rocks formed in oceanic island arcs that have low Th/Yb (0.05–1.0) and Ta/Yb (0.02–1.0) ratios, indicating a Th and Ta enrichment by the interaction of the melts with continental crust. The mafic granulites of the Ongole domain have moderate ratios of Th/Yb (0.12–1.38, average 0.63) and high Ta/Yb (0.12–0.30, average 0.21). The Th/Yb values fall in the range of oceanic island arcs, while the Ta/Yb ratios lie at the lower end of the range for active continental margins (Fig. 8c). This suggests that the role of crustal contamination during the formation of the precursor magmas is minor.

Petrogenesis of the charnoenderbites

The charnoenderbites of the Ongole domain have variable SiO_2 content (52.2–72.5 wt%) and display negative correlations between SiO_2 and MgO, Fe_2O_3, CaO, Ni and Cr and a positive correlation with K_2O. The large variation in SiO_2 and the element correlations are best explained by magma differentiation. Lower values of Cr and Ni than that of the mafic granulites can be explained by extensive fractionation of pyroxene (Fig. 4e, f). In the plot of Fe* against wt% SiO_2 and $Na_2O + K_2O$–CaO against wt% SiO_2 (Fig. 3b, c), the similarity of the charnoenderbites and the Cordilleran granitoids of USA suggests that these rocks were formed by similar petrogenetic processes. Most zircon grains of charnoenderbite samples display resorption of oscillatory-zoned old magmatic cores and subsequent growth of metamorphic rims (see section 'U–Pb zircon geochronology'). So we think that Zr was locally remobilized but did not affect the Zr concentration of the bulk rock.

In addition, the charnoenderbites show a pronounced Nb–Ta depletion (Nb/La_{pm} = 0.04–0.45, mean 0.26; Ta/La_{pm} = 0.06–0.44, mean 0.19) relative to the other incompatible elements (Fig. 5d) that are typical of rocks formed in a magmatic arc setting and is primarily due to the preferential retention of the two elements by mineral phases like rutile and ilmenite. This argument is in agreement with the low contents of TiO_2 (0.1–2.1 wt%, mean 0.75).

Similar to the mafic granulites, the charnoenderbites are also characterized by highly enriched LREE (La/Yb_{CN} = 4.2–71.1) relative to HREE (Fig. 5c), which shows moderate depletion (Tb/Yb_{CN} = 1.1–3.0). In the Sr/*Y* vs. *Y* plot (Drummond and Defant 1990; Fig. 8a) and La/Yb_{CN} vs. Yb_{CN} plot (Martin 1986; Fig. 8b), the charnoenderbites lie in the field of typical island arc rocks. The charnoenderbite suite also plots mainly in the volcanic arc granite field of the Rb vs. Y+Nb diagram (Pearce et al. 1984; Fig. 8e).

There are three distinct low *Y* charnoenderbites with very low *Y* (1.8–2.5 ppm) and Yb (0.22–0.46 ppm) contents and plotting in the field of adakites in the Sr/*Y* vs. *Y* and La/Yb_{CN} vs. Yb_{CN} diagrams (Fig. 8a, b). The fact that Sr/*Y* and La/Yb_{CN} are similarly high suggests that Sr/*Y* ratios largely reflect magmatic compositions. The name 'adakite' is used to describe a large group of rocks whose sole feature is high Sr/*Y* and La/Yb_{CN} ratios (Moyen 2009). The original adakites, as defined by Defant and Drummond (1990) and termed as 'high silica adakites' by Martin et al. (2005), have characteristic chemical composition (SiO_2 > 56 %, Al_2O_3 > 15 %, MgO > 3.5 %, K_2O/Na_2O < 0.5, *Y* and Yb < 18 and 1.9 ppm and Sr > 400 ppm). The genesis of these high silica adakites is best explained by the classical 'slab melting' model, where the melts are interpreted to have formed by partial melting of the subducting slab leaving garnet ± amphibole as residual phases, which preferentially retain HREE and *Y*, producing depletion in the magma. But, as plagioclase is not a residual phase, the magmas lack a negative Eu anomaly. However, there is a growing evidence that the sole signature of high Sr/*Y* and La/Yb_{CN}, by which the term adakite is defined, can be achieved through different processes than slab melting, but in these cases, the rocks lack the other chemical characteristics of 'high silica adakites' (Moyen 2009). They may form in geodynamic settings not typically associated with active subduction, as well as in a subduction setting, but not necessarily related to slab melts. For example, the adakites can form through differentiation and/or partial melting

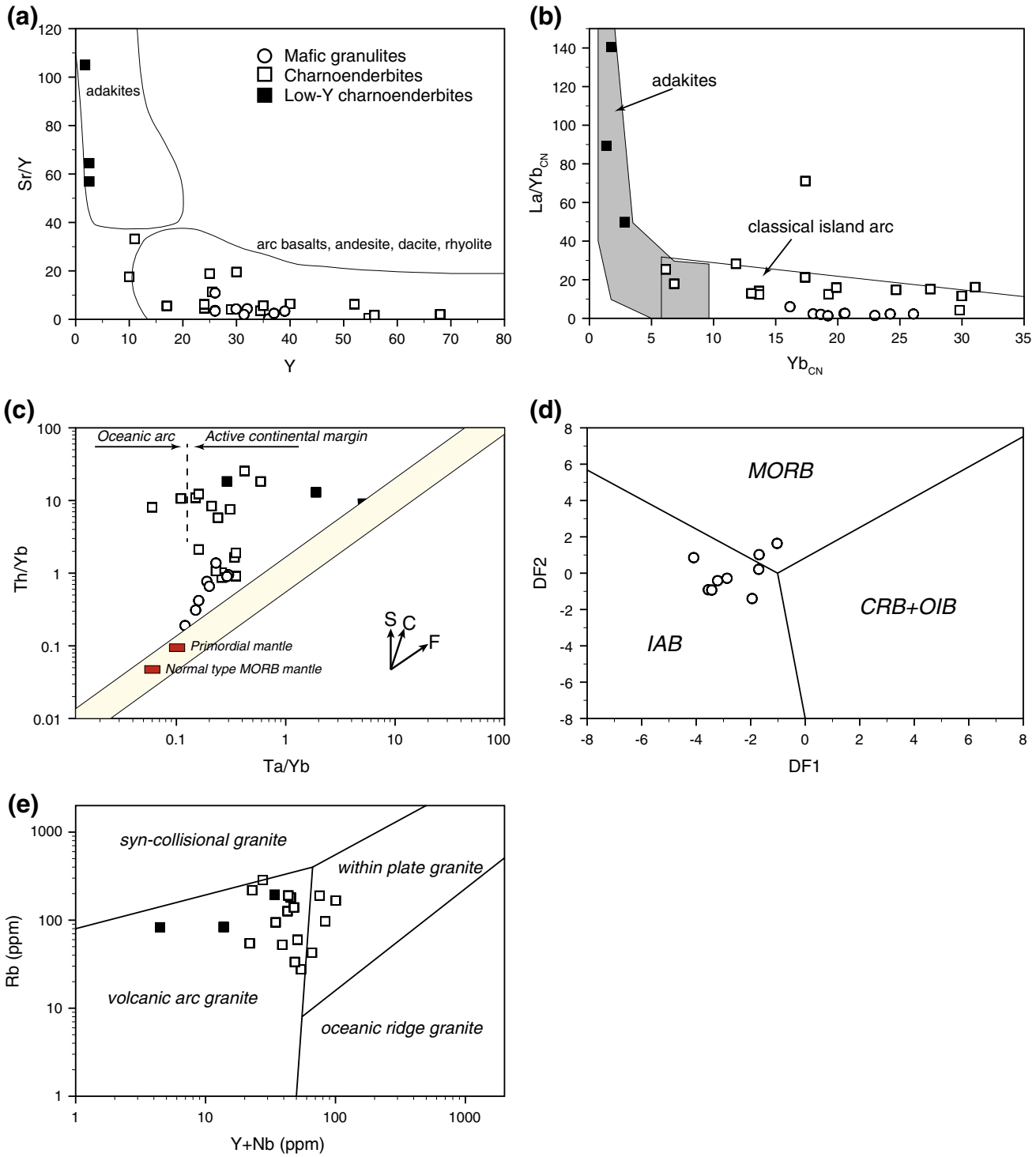

Fig. 8 The Sr/*Y* vs. *Y* plot (modified from Defant and Drummond, 1990) and **b** the La/Yb$_{CN}$ vs. Yb$_{CN}$ plot of Martin 1986 for the magmatic rocks of the Ongole domain; **c** basaltoid tectonic discrimination diagram modified from Pearce (1983). S = subduction zone enrichment trend, C = crustal contamination trend, *F* = fractional crystallization trend (*F* = 0.5); **d** log-transformed basaltoid discrimination diagram modified from Agrawal et al. (2008). DF1 = 0.3518 Log(La/Th) + 0.6013 Log(Sm/Th) − 1.3450 Log(Yb/Th) +2.1056 Log(Nb/Th) − 5.4763; and DF2 = −0.3050 Log(La/Th) − 1.1801 Log(Sm/Th) +1.6189 Log(Yb/Th) + 1.2260 Log(Nb/Th) − 0.9944. MORB = mid-ocean ridge basalts, IAB = island arc basalt, CRB = continental rift basalt, OIB = ocean island basalt; **e** Rb vs. Y + Nb granitoid tectonic discrimination diagram of Pearce et al. 1984

processes at the base of an arc crust (Bindeman et al. 2005) or are produced by fractional crystallization of garnet-bearing assemblages from metasomatized mantle-derived basaltic arc magmas (Macpherson et al. 2006). However, in all cases, garnet plays the most important role in fractionating HREE and *Y*. The three low *Y* charnoenderbites that plot in the field of adakites are different from the composition of 'high silica adakites.' Therefore, these three rocks are not likely to be produced by slab melts. Instead, one possibility is that they were produced by partial melting of older continental crust in a subduction zone setting where garnet was stable. A second possibility is that the rocks formed from melts undergoing deep crustal magmatic differentiation when garnet was a stable phase. Garnet can retain HREE and *Y* and producing similar trace element patterns in the fractionated melt. High Sr/*Y* ratios, low HREE and *Y* contents, coupled with positive Eu anomaly, can also result from the early amphibole fractionation (incorporated HREE and *Y* relative to Sr) and plagioclase retention (Dessimoz et al. 2012). Thus, it is not necessary to fractionate garnet in order to obtain Sr-rich, *Y*- and HREE-depleted rocks. However, amphibole is stabilized rather than plagioclase due to high water content in the melt, and igneous amphibole is normally present in the plutonic rocks of those suites (Dessimoz et al. 2012). High H_2O content in the melts is in conflict with the complete absence of amphibole relicts in the charnoenderbites and the presence of Opx, which requires low H_2O activity. Although Opx could have formed only during metamorphism, the absence of amphibole in the rocks suggests that garnet fractionation is more likely in producing the HREE-depleted trends. In the absence of other isotopic data to distinguish between juvenile melts fractionated in deep arc crust (in the presence of garnet or amphibole) or partial melting of older continental crust, either of the possibilities might apply. Both these interpretations are consistent with the genesis of the spatially and temporally associated rocks in a magmatic arc setting.

Incompatible trace element ratios (e.g., Th/Yb and Ta/Yb) are useful in investigating crustal contamination of mantle-derived melts (Pearce 1983). The charnoenderbites of the Ongole domain have high and variable ratios of Th/Yb (1.1–25.5) and high Ta/Yb (0.1–0.6) ratios that fall in the range defined for active continental margins (Fig. 8c; Pearce 1983). This suggests that there is minor crustal contamination in the trace element signatures of the charnoenderbites. This interpretation is in agreement with the observation that migmatitic metapelites form enclaves within the charnoenderbites. Crust–magma interaction is typical of continental arcs and can explain some of the trace element signatures such as enriched LREE and high Th/Nb ratios.

Geodynamic setting

Based on the geological, geochronological and geochemical evidence presented above, we propose that the Ongole domain was formed as a subduction-related magmatic arc during the Paleoproterozoic. The arc was situated near the continental margin of the Eastern Dharwar craton with a remnant oceanic basin in between the arc and the continent (Fig. 9a). This basin was most likely the site of deposition of continental sediments derived from the felsic granitoids of the adjacent Eastern Dharwar craton. This is highlighted by the Nd model ages (T_{DM}) of the migmatitic metapelites (2.8–2.6 Ga) reflecting the mean crustal residence age of the provenance areas, which are similar to the Nd model ages of the granitoids of the Eastern Dharwar craton (Rickers et al. 2001).

The oceanic slab dehydrated before melting and releasing aqueous fluids that rose and metasomatized the overlying mantle wedge. The fluids triggered partial melting of the mantle peridotite, which generated the parental magma of the mafic granulites (Fig. 9a). These juvenile magmas ascended through the mantle and were probably emplaced at the base of the crust and slightly contaminated resulting in Ta/Yb ratios higher than that of rocks formed in an oceanic island arc. Subsequent differentiation of the basic magma led to the formation of intermediate to felsic parental magmas of the charnoenderbites. Owing to their buoyancy, they moved upwards incorporating enclaves of basic and metasedimentary rocks. These processes resulted in widespread volcanism and plutonism in the Ongole domain between 1,750 and 1,710 Ma (Fig. 9a). Nd model ages of 2.5–2.3 Ga for the charnoenderbites (Rickers et al. 2001) also argue for the contamination with older crustal sediments. Unfortunately, ages reflecting this syn-magmatic metamorphism were not found in zircon grains of the metapelitic enclaves (Sarkar et al. 2014). However, Nd model ages of the charnoenderbites that are 600–800 million years older than the intrusive ages documented in this study open the possibility for alternative geodynamic interpretations. The arc signature seen in these intrusive meta-igneous rocks could equally be inherited from older continental crust (late Archean), which itself formed by arc accretion, and then re-melted to form the charnoenderbites. This process would also generate rocks with intrusive ages younger than the Nd model ages, but at the same time, some zircon grains from the older crust are most likely to be incorporated in the newly generated melt and would act as seeds for new zircon growth. But inherited zircon cores were not found in a single zircon grain from the several charnoenderbites that have been dated. Though this lack of evidence does not completely exclude the possibility of crustal remelting, it favors the interpretation of juvenile

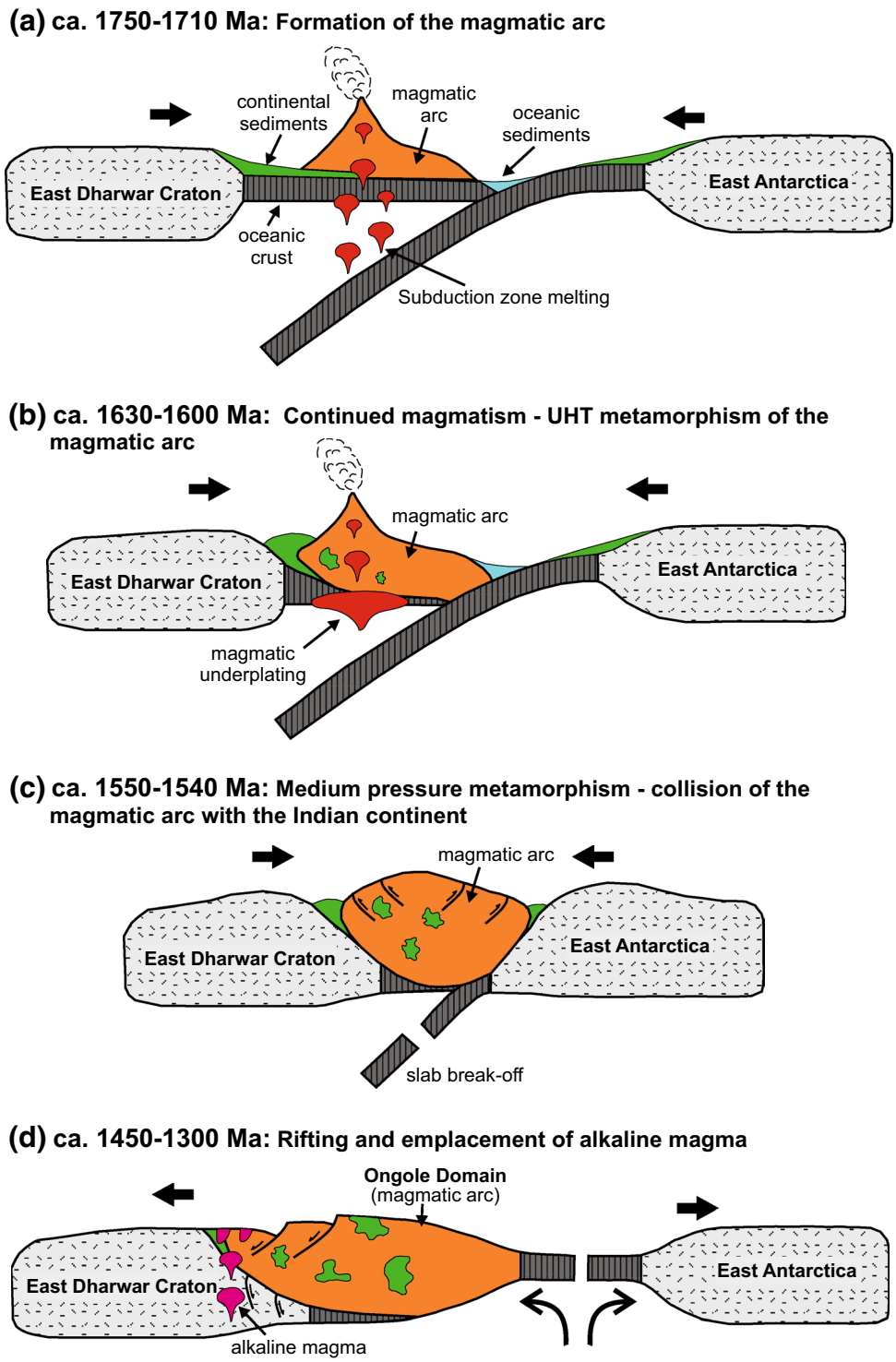

Fig. 9 Model showing sequences of tectonic evolution of the Ongole domain (simplified after Dasgupta et al. 2013) with constraints from new geochronological data. See text for details of the sequences **a** to **d**

melts. Further isotopic studies (e.g., O and Hf isotope data of the zircons to test their juvenility) are required to resolve this issue. Due to the complete absence of inherited zircon cores in all dated charnoenderbites and based on the argument of field relationships (i.e., incorporated migmatitic metapelites in charnoenderbite), we prefer the model of a juvenile arc undergoing crustal contamination with older continental sediments, explaining Nd model ages older than the intrusive ages.

The presence of a ca. 1,750–1,700 Ma old magmatic arc in the Eastern Ghats Belt is critical in understanding the accretionary history of supercontinent Columbia, which formed at ca. 2.1–1.8 Ga (Zhao et al. 2002; Rogers and Santosh 2002). Columbia is believed to have undergone a

long lived (1.8–1.2 Ga) subduction-related episodic growth due to the accretion along some of its continental margin involving Laurentia, Baltica, South America, Australia and China (Zhao et al. 2004). Petrological and geochemical studies indicate that the large accretionary magmatic belts include juvenile volcanogenic sequences and granitoid suites resembling those of present day magmatic arcs (Zhao et al. 2004). Bose et al. (2011) proposed to include the SE margin of India as an accretionary magmatic belt during Columbia formation based on geochronological constraints. This is in agreement with our geochronological and geochemical data.

The period of ca. 1,710–1,630 Ma was probably a period of quiescence as evidence for major tectonothermal activity is absent. Reactivation of subduction processes led to mafic magmatism inducing UHT metamorphism at low pressures between ca. 1,630 and 1,600 Ma (Fig. 9b). The heat from mafic magmas resulted in remelting of some older rocks and emplacement of felsic magmas during metamorphism (Fig. 9b). Subsequent to subduction of the back-arc basin, arc-continent collision resulted in a thickened crust and the rocks experienced a higher-pressure lower-temperature second metamorphism dated at ca. 1,540 Ma (Fig. 9c). The evolution of the Ongole magmatic arc has similarities with the Areachap magmatic arc in South Africa, which magmatically grew until ca. 1,240 Ma and was juxtaposed with the craton at ca. 1,200 Ma (Pettersson et al. 2007). The overall compressional history in the Ongole domain changed to extension dominated tectonics at ca. 1,450 Ma with the opening of an ocean basin (Upadhyay 2008) and emplacement of alkaline rocks in a rift setting along the craton-mobile belt contact (Fig. 9d). Thus, all the tectonothermal events including the UHT metamorphism are considered to be a part of this accretionary process during the growth of the Paleo-Mesoproterozoic supercontinent Columbia.

Conclusions

Based on field observations, U–Pb zircon geochronology and geochemical data presented in this paper, we draw the following conclusions.

(1) U–Pb zircon ages indicate that a widespread magmatic activity in the Ongole domain started in the Paleoproterozoic at ca. 1,750 Ma resulting in the emplacement of evolved calc-alkaline granitoids and some mafic rocks. The magmatic activity lasted for ca. 40 Ma giving rise to different generations of magmatic rocks having complex crosscutting field relationships.
(2) The Paleoproterozoic magmatic rocks preserve trace and rare earth element characteristics that are analogous to modern day continental arcs.
(3) These magmatic rocks along with metapelitic enclaves experienced a high-grade (UHT) metamorphism during the late Paleoproterozoic (ca. 1,610 Ma) attributed to further magmatic activities. This was followed by a second metamorphism at lower temperatures but higher pressures during early Mesoproterozoic (ca. 1,540 Ma), marking the collision of the magmatic arc with the Indian continent.

Acknowledgments The authors would like to thank Prof. J. Erzinger for generously extending the geochemical laboratory facilities at GeoForschungsZentrum in Potsdam and S. Tonn and H. Rothe for their help with geochemical analysis. We extend our thanks to Prof. M. Raith for providing geochemical data of six samples from the Ongole domain and for his insightful discussions. We sincerely thank O. Müntener for his efficient editorial handling and the three anonymous reviewers for their critical but very constructive comments, which have undoubtedly improved the quality of the manuscript.

References

Agrawal S, Guevara M, Verma SP (2008) Tectonic discrimination of basic and ultrabasic volcanic rocks through log-transformed ratios of immobile trace elements. Int Geol Rev 50:1057–1079. doi:10.2747/0020-6814.50.12.1057

Arndt N (2013) Formation and evolution of the continental crust. Geochem Perspect 2:405–533. doi:10.7185/geochempersp.2.3

Bindeman IN, Eiler JM, Yogodzinski GM et al (2005) Oxygen isotope evidence for slab melting in modern and ancient subduction zones. Earth Planet Sci Lett 235:480–496. doi:10.1016/j.epsl.2005.04.014

Bose S, Dunkley DJ, Dasgupta S et al (2011) India–Antarctica–Australia–Laurentia connection in the Paleoproterozoic–Mesoproterozoic revisited: evidence from new zircon U-Pb and monazite chemical age data from the Eastern Ghats Belt, India. GSA Bull 123:2031–2049. doi:10.1130/B30336.1

Cawood PA, Kröner A, Pisarevsky S (2006) Precambrian plate tectonics: criteria and evidence. GSA Today 16:4–11

Condie KC (2000) Episodic continental growth models: afterthoughts and extensions. Tectonophys 322:153–162

Dasgupta S, Bose S, Das K (2013) Tectonic evolution of the Eastern Ghats Belt, India. Precam Res 227:247–258

Defant MJ, Drummond MS (1990) Derivation of some modern arc magmas by melting of young subducted lithosphere. Nature 347:662–665

Dessimoz M, Müntener O, Ulmer P (2012) A case for hornblende dominated fractionation of arc magmas: the chelan complex (Washington Cascades). Contrib Miner Petrol 163:567–589

Dharma Rao CV, Santosh M (2011) Continental arc magmatism in a Mesoproterozoic convergent margin: petrological and geochemical constraints from the magmatic suite of Kondapalle along the eastern margin of the Indian plate. Tectonophys 510:151–171. doi:10.1016/j.tecto.2011.06.025

Dharma Rao CV, Santosh M, Dong Y (2012) U-Pb zircon chronology of the Pangidi-Kondapalle layered intrusion, Eastern Ghats Belt, India: constraints on Mesoproterozoic arc magmatism in a convergent margin setting. J Asian Earth Sci 49:362–375. doi:10.1016/j.jseaes.2011.07.005

Dobmeier CJ, Raith MM (2003) Crustal architecture and evolution of the Eastern Ghats Belt and adjacent regions of India. Geol Soc Spec Pub Lond 206:145–168

Drummond MS, Defant MJ (1990) A model for Trondhjemite-Tonalite-Dacite Genesis and crustal growth via slab melting: archean to modern comparisons. J Geophys Res 95:21503–21521. doi:10.1029/JB095iB13p21503

Dulski P (2001) Reference materials for geochemical studies: new analytical data by ICP-MS and critical discussion of reference values. Geostand Newsl 25:87–125

Frost BR, Barnes CG, Collins WJ et al (2001) A geochemical classification for granitic rocks. J Petrol 42:2033–2048

Govindaraju K (1994) 1994 compilation of working values and sample description for 383 geostandards. Geostand Newsl 18:1–158. doi:10.1046/j.1365-2494.1998.53202081.x-i1

Hawkesworth CJ, Kemp AIS (2006) Evolution of the continental crust. Nature 443:811–817. doi:10.1038/nature05191

Irvine T, Baragar W (1971) A guide to the chemical classification of the common volcanic rocks. Canad J Earth Sci 8:523–548

Jackson SE, Pearson NJ, Griffin WL, Belousova EA (2004) The application of laser ablation-inductively coupled plasma-mass spectrometry to in situ U-Pb zircon geochronology. Chem Geol 211:47–69

Jagoutz O, Muentener O, Ulmer P, Pettke T, Burg JP, Dawood H, Hussain S (2007) Petrology and mineral chemistry of lower crustal intrusions: the chilas complex, Kohistan (NW Pakistan). J Petrol 48:1895–1953. doi:10.1093/petrology/egm044

Kelemen PB, Hanghøj K, Greene AR (2003) One view of the geochemistry of subduction-related magmatic arcs, with an emphasis on primitive andesite and lower crust. In: Rudnick RL (ed) Treatise on geochemistry. Elsevier, Oxford, pp 593–659

Kooijman E, Berndt J, Mezger K (2012) U-Pb dating of zircon by laser ablation ICP-MS: recent improvements and new insights. Eur J Miner 24:5–21. doi:10.1127/0935-1221/2012/0024-2170

Korsch RJ, Kositcin N, Champion DC (2011) Australian island arcs through time: geodynamic implications for the Archean and Proterozoic. Gond Res 19:716–734. doi:10.1016/j.gr.2010.11.018

Kovach VP, Simmat R, Rickers K et al (2001) The western charnockite zone of the Eastern Ghats Belt, India-an independent crustal province of late Achaean (2.8 Ga) and Palaeoproterozoic (1.7–1.6 Ga) terrains. Gond Res 4:666–667. doi:10.1016/S1342-937X(05)70462-7

Le Bas MJ, Le Maitre RW, Streckeisen A, Zanettin B (1986) A chemical classification of volcanic rocks based on the total alkali-silica diagram. J Petrol 27:745–750

Liang Q, Grégoire DC (2000) Determination of trace elements in twenty six chinese geochemistry reference materials by inductively coupled plasma-mass spectrometry. Geostand Newsl 24:51–63

Macpherson CG, Dreher ST, Thirlwall MF (2006) Adakites without slab melting: high pressure differentiation of island arc magma, Mindanao, the Philippines. Earth Planet Sci Lett 243:581–593. doi:10.1016/j.epsl.2005.12.034

Martin H (1986) Effect of steeper Archean geothermal gradient on geochemistry of subduction-zone magmas. Geology 14:753–756

Martin H, Smithies RH, Rapp R, Moyen JF (2005) An overview of adakite, tonalite–trondhjemite–granodiorite (TTG), and sanukitoid: relationships and some implications for crustal evolution. Lithos 79:1–24

McDonough WF, Sun SS (1995) The composition of the earth. Chem Geol 120:223–253

Moyen J-F (2009) High Sr/Y and La/Yb ratios: the meaning of the adakitic signature. Lithos 112:556–574. doi:10.1016/j.lithos.2009.04.001

Pearce JA (1983) Role of the sub-continental lithosphere in magma genesis at active continental margins. In: Hawkesworth CJ, Norry MJ (eds) Continental basalts and mantle xenoliths. Shiva Press Limited, Cheshire, pp 230–249

Pearce JA, Cann JR (1973) Tectonic setting of basic volcanic rocks determined using trace element analyses. Earth Planet Sci Lett 19:290–300. doi:10.1016/0012-821X(73)90129-5

Pearce JA, Peate DW (1995) Tectonic implications of the composition of volcanic arc magmas. Ann Rev Earth Planet Sci 23:251–286

Pearce JA, Harris NBW, Tindle AG (1984) Trace element discrimination diagrams for the tectonic interpretation of granitic rocks. J Petrol 25:956–983

Pettersson Å, Cornell DH, Moen HFG et al (2007) Ion-probe dating of 1.2 Ga collision and crustal architecture in the Namaqua-Natal Province of southern Africa. Precamb Res 158:79–92. doi:10.1016/j.precamres.2007.04.006

Polat A (2012) Growth of Archean continental crust in oceanic island arcs. Geology 40:383–384. doi:10.1130/focus042012.1

Ramakrishnan M, Nanda JK, Augustine PF (1998) Geological evolution of the Proterozoic Eastern Ghats mobile belt. Geol Sur India Spec Pub 44:1–21

Ravikant V, Kröner A, Vasudevan D, Wendt I, Tobschall H, Chatterjee C (2013) Zircon evaporation ages and geochemistry of metamorphosed volcanic rocks from the Vinjamuru domain, Krishna Province: evidence for 1.78 Ga convergent tectonics along the southeastern margin of the Eastern Dharwar Craton. Geol J 48:293–309

Rickers K, Mezger K, Raith MM (2001) Evolution of the continental crust in the Proterozoic Eastern Ghats Belt, India and new constraints for Rodinia reconstruction: implications from Sm–Nd, Rb–Sr and Pb–Pb isotopes. Precamb Res 112:183–210

Rogers JJW, Santosh M (2002) Configuration of Columbia, a Mesoproterozoic supercontinent. Gond Res 5:5–22. doi:10.1016/S1342-937X(05)70883-2

Rudnick RL (1995) Making continental crust. Nature 378:571–578

Sarkar T, Schenk V (2014) Two-stage granulite formation in a Proterozoic magmatic arc (Ongole domain of the Eastern Ghats Belt, India): part 1. Petrology and pressure-temperature evolution. Precam Res 255:485–509

Sarkar T, Schenk V, Appel P, Berndt J, Sengupta P (2014) Two-stage granulite formation in a Proterozoic magmatic arc (Ongole domain of the Eastern Ghats Belt, India): part 2. LA-ICP-MS zircon dating and texturally controlled in situ monazite dating. Precam Res 255:467–484

Şengör AMC, Natal'in BA, Burtman VS (1993) Evolution of the Altaid tectonic collage and Palaeozoic crustal growth in Eurasia. Nature 364:299–307. doi:10.1038/364299a0

Sengupta P, Sen J, Dasgupta S et al (1999) Ultra-high temperature metamorphism of metapelitic granulites from Kondapalle, Eastern Ghats Belt: implications for the Indo-Antarctic correlation. J Petrol 40:1065–1087

Simmat R, Raith MM (2008) U–Th–Pb monazite geochronometry of the Eastern Ghats Belt, India: timing and spatial disposition of poly-metamorphism. Precamb Res 162:16–39

Sun SS, McDonough WF (1989) Chemical and isotopic systematics of oceanic basalts: implications for mantle composition and processes. Geol Soc Lond Spec Pub 42:313–345. doi:10.1144/GSL.SP.1989.042.01.19

Taylor SR, McLennan SM (1985) The continental crust: its composition and evolution. Blackwell Scientific Publications, Oxford, pp 1–312

Upadhyay D (2008) Alkaline magmatism along the southeastern margin of the Indian shield: implications for regional geodynamics and constraints on craton–Eastern Ghats Belt suturing. Precamb Res 162:59–69

Wiedenbeck M, Alle P, Corfu F, Griffin WL, Meier M, Oberli F, Von Quadt A, Roddick JC, Spiegel W (1995) Three natural zircon

standards for U–Th–Pb, Lu–Hf, trace element and REE analyses. Geostand Newsl 19:1–23

Windley BF, Garde AA (2009) Arc-generated blocks with crustal sections in the North Atlantic craton of West Greenland: crustal growth in the Archean with modern analogues. Earth Sci Rev 93:1–30. doi:10.1016/j.earscirev.2008.12.001

Zhao G, Cawood PA, Wilde SA, Sun M (2002) Review of global 2.1–1.8 Ga orogens: implications for a pre-Rodinia supercontinent. Earth Sci Rev 59:125–162

Zhao G, Sun M, Wilde SA, Li S (2004) A Paleo-Mesoproterozoic supercontinent: assembly, growth and breakup. Earth Sci Rev 67:91–123. doi:10.1016/j.earscirev.2004.02.003

Zuleger E, Erzinger J (1988) Determination of the REE and Y in silicate materials with ICP-AES. Fresenius J Anal Chem 332:140–143